Determination of the Optical Properties of a Paperboard Packaging Material for Laser Applications

Master's Thesis
by
Anette Nordström

Tetra Pak Packaging Solutions AB
Development & Engineering
And
Atomic Physics Division
Lund Institute of Technology
Lund, March 2007

Abstract

Tetra Pak is a world leading company in the packaging industry, constantly working to develop new packaging techniques. To be able to involve lasers in the packaging process, makes it necessary to understand how light interacts with the packaging material, paperboard.

The purpose with this thesis is to investigate paperboard in terms of optical properties in the wavelength region of interest. It is also desirable to investigate how the paperboard can be treated to change the optical properties.

In this thesis two cases are investigated, pure paperboard samples and paperboard treated with mineral oil. The investigation is done by firstly determining the transmission and reflection of the samples with an integrating sphere, followed by the evaluation of the optical properties by the IAD program, resulting in the scattering and absorption coefficients of the paperboard. Difficulties with this determination were the layered structure of the samples, consisting of both white and brown paperboard. To describe how the laser light propagates through the paperboard two models are applied; Diffusion theory and a Monte Carlo convolution method. Finally experiments were performed with the aim to verify the light propagation models.

The results from the simulations showed good agreement with the integrating sphere measurements, indicating that the evaluated optical coefficients are a valid approximation.

Contents

Chapter 1 Introduction

1.1 Background

Tetra Pak is a world leading company in the industry of processing and packaging of different foods. In the beginning it was only packaging of liquid foods but that has been expanded to also include ice cream, cheese and fruits to name a few. Since the early 1990s when Tetra Pak purchased Alfa Laval with their liquid process technology, Tetra Pak has been able to offer their customers processing of their liquid food before packaging it. Nowadays, more and more customers are taking advantage of Tetra Pak's ability to provide complete plant solutions, from product reception right through to final packaging in carton and plastic containers, all from a single source.

Tetra Pak is constantly working to develop new packaging techniques that are consistent with the key phrase "A package should save more than it costs". This phrase is applied to both the economic and environmental performance of the packaging systems. The main component of the packages, namely paperboard, is definitely measuring up to both aspects.

Tetra Pak now wants to involve lasers in the packaging process, which makes it necessary to understand how light interacts with a paperboard material.

1.2 Purpose

The purpose of this Master's thesis is to enhance the understanding of light propagation through paperboard for laser applications, and how the paperboard can be treated to change these properties.

Realistic samples are manufactured to mirror the actual situation, which includes different surface treatments as well as a substance added to the paperboard. The different cases are investigated in terms of their impact on the transmission.

1.3 Scope of thesis

The thesis work includes:

1. Integrating sphere measurements which result in obtaining the transmission and reflection of the paperboard samples.

2. Inverse adding-doubling simulations which yield the optical parameters of the paperboard samples given the results from the integrating sphere measurements.

3. Monte Carlo simulations to verify the parameters from the Inverse adding-doubling simulations.

4. Power and temperature measurements on the samples with a diode laser.

5. The development of a model that describes the light propagation through the paperboard.

6. A comparison between the parameters obtained from the simulations, the experimental work and the mathematical model.

The samples have different surface treatments and are investigated in terms of their impact on the transmission, both in the untreated case as well the case with mineral oil added to the paperboard.

1.4 Outline

The thesis starts with a theory chapter which includes light propagation and optical properties of turbid media, the application of Beer-Lambert's law, the transport equation and different ways to solve it and also the principle of laser action as well as a description of the diode laser. Chapter 3 gives a description of the investigated samples and the performed measurements and simulations. The results of the measurements, simulations and the model used to describe light propagation are presented chapter 4. This chapter also includes a discussion and comparison of the results. Finally, the conclusions are presented in chapter 5. Appendix A gives the Matlab code for the diffusion model and in Appendix B a summary in Swedish is found.

Chapter 2 Theory

This chapter treats light propagation and different ways to model it, as well as the principles of lasers and the diode laser in particular.

2.1 Light propagation in scattering media

When light interacts with material, the light is either absorbed or scattered in different directions. How this interaction occurs depends on the optical properties of the material and is also dependent on the wavelength of the incident light.

2.1.1 Optical properties

The following section gives the theory behind the different parameters used to describe a material in terms of optical properties.

Reflection
There is always a reflection in the surface between two media with different refractive indices, which is shown in figure 2.1. Other influential factors are structure and shape of the surface and light polarisation. If polarisation is neglected, the reflected fraction R is governed by Fresnel's law, equation 2.1.

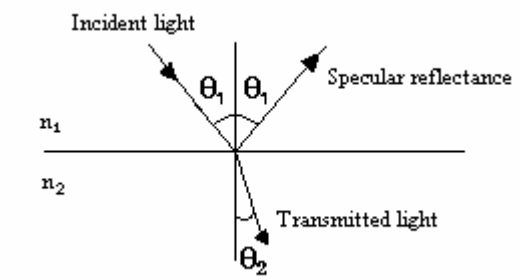

Figure 2.1. Schematic picture of the reflection in a surface due to the mismatch of the refractive index.[1]

$$R = \frac{1}{2}\left[\frac{\tan^2(\theta_1 - \theta_2)}{\tan^2(\theta_1 + \theta_2)} + \frac{\sin^2(\theta_1 - \theta_2)}{\sin^2(\theta_1 + \theta_2)}\right] \qquad (2.1)$$

Here θ_1 is the angle of incidence and the angle θ_2 is given by Snell's law, where n_1 and n_2 is the refractive indices of the different layers.

$$n_1 \cdot \sin\theta_1 = n_2 \cdot \sin\theta_2 \qquad (2.2)$$

[1] A. J. Welch, M. J. C. van Gemert (1995)

If the beam is perpendicular to the surface, Fresnel's law is reduced to equation 2.3 and this represents the reflection minimum.

$$R = \frac{(n_1 - n_2)^2}{(n_1 + n_2)^2} \tag{2.3}$$

Scattering and absorption
A photon gets absorbed by a molecule if its energy corresponds to the energy difference between two electronic states in the molecule. The absorption coefficient μ_a is used to describe how much a material is absorbing and gives the probability for absorption per unit path length. It is often given in cm^{-1}. The absorption coefficient is governed by the concentration of absorbing particles in the sample.

The scattering process can be divided into two groups, the elastic and the inelastic scattering. Inelastic scattering gives an energy shift between the incident and scattered light, whereas the elastic scattering doesn't. From now on, only elastic scattering is considered.

Mathematically the scattering is described by Rayleigh theory when the scattering particles are very small compared to the light wavelength and by Mie theory when the particles are of comparable size to the wavelength. The wavelength dependency is about λ^{-4} for Rayleigh scattering and λ^{-n}, where n varies between approximately between 1 and 2 dependent on the relative size between the scatterer and the wavelength of the light for Mie scattering. This means that shorter wavelengths gets more scattered than longer wavelengths, which is especially apparent for Rayleigh scattering because of the stronger wavelength dependence.[2]

To describe the scattering property of a material the scattering coefficient μ_s is used, and similar to the absorption coefficient, it describes the probability of a photon being scattered per unit path length.

The absorption and scattering coefficients can be summarised into the attenuation coefficient.

$$\mu_t = \mu_a + \mu_s \tag{2.4}$$

Anisotropy factor and phase function
Besides from the above mentioned coefficients there is a third property that is used to describe light-material interaction; the anisotropy factor g. This factor describes the direction of the scattering.

The scattering angle from a single scattering event has a probability distribution called the phase function, $p(\hat{s}, \hat{s}')$. The phase function describes the probability that light travelling in a direction $\hat{s}$ will be scattered into the direction $\hat{s}'$. This probability

[2] C. af Klinteberg (1999)

distribution is symmetric about the direction of incidence for most tissues. It can also be expressed as a function of the angle θ between $\hat{s}'$ and $\hat{s}$.

$$p(\hat{s},\hat{s}') = p(\cos\theta) \tag{2.5}$$

The total scattering probability equals one

$$\int_{4\pi} p(\hat{s},\hat{s}')d\omega' = 1 \tag{2.6}$$

The anisotropy factor is defined as the mean cosine of the scattering angle, se equation 2.5. It can have values between -1 and 1, where g= -1 means backscattering, g= 0 isotropic scattering and g= 1 forward scattering.

$$g = \int_{4\pi} \cos\theta \cdot p(\cos\theta)d\omega \tag{2.7}$$

When the anisotropy factor and the scattering coefficient can not be separately determined, the reduced scattering coefficient is used.

$$\mu_s' = (1-g)\mu_s \tag{2.8}$$

2.1.2 Beer-Lambert's Law

Light, of any wavelength, with the intensity I_0 impinging on a sample of thickness z, will be attenuated when passing the sample if the sample interacts with the light. During a length interval Δx the intensity will decrease with ΔI. The fractional attenuation ΔI/I will be proportional to the number of absorbers, Δn, in the small interval Δx.

$$\frac{\Delta I}{I} = -k\Delta n = -k_1 c\Delta x \tag{2.9}$$

k and k_1 are constants and the last equality is valid for a sample with a uniform concentration of absorbers, c, through the sample. Integration of equation 2.9 yields an expression for the intensity as a function of depth.

$$\int_{I_0}^{I} \frac{dI}{I} = -\int_0^N kdn = -\int_0^d k_1 c dx\,,\ \ln\frac{I_0}{I} = kN = k_1 cd \Rightarrow\ I = I_0 e^{-k_1 cd} \tag{2.10}$$

This is the Beer-Lambert law that states that the absorbance is proportional to the concentration c [mol/m^3] of absorbers in the sample.[3] If a sample was only absorbing, the transmitted light could be described by Beer-Lambert's law where the attenuation coefficient $\mu_t = \mu_a + \mu_s$ is recognised.

[3] S. Svanberg (2004)

$$E(z) = E_0(1-r)e^{-(\mu_a+\mu_s)z} \quad , \mu_s = 0 \qquad (2.11)$$

E(z) is the fluence rate of the collimated transmittance at position z, E_0 is the collimated irradiance and r is the specular reflectance defined in equation 2.1.

To determine the attenuation coefficient, the natural logarithm of the collimated transmittance, ln T_c, is plotted versus the thickness z; the coefficient is obtained from the slope of the curve.

$$\ln T_c = \ln\left[\frac{E(z)}{E_0}\right] = \ln(1-r) - \mu_t z \qquad (2.12)$$

Experimentally it is difficult to separate the collimated transmittance from scattered light, which will result in uncertainties in the obtained attenuation coefficient.

2.2 Theoretical models

Light transport can be modelled by an analytical theory based on transport theory.

An analytical wave model describes the light propagation as a continuous transfer of energy by electromagnetic waves and starts from basic differential equations like Maxwell's equations or the wave equations. This approach is mathematically rigorous since it in principle includes all the multiple scattering, diffraction and interference effects.

In transport theory the light propagation is treated as a stream of particles- photons, which each has a specific amount of energy. The mathematical description is a statistical approximation of energy transport through a turbid medium. This theory only considers transport of power and wave phenomenon like polarisation, interference and diffraction are neglected.[4]

2.2.1 Transport equation

The radiative transport equation, RTE, is built up by five different contributions, as described schematically in figure 2.2. The equation is expressed as a continuity function of the radiance, L, that is the light intensity per unit area and solid angle, as defined in equation 2.13.

$$L(\bar{r},\hat{s}) = N(\bar{r},\hat{s})h\nu c \qquad [\mathrm{W/m^2 \cdot sr}] \qquad (2.13)$$

$N(\bar{r},\hat{s})$ describes the number of photons at point r, moving in the direction $\hat{s}$ with the velocity c and $h\nu$ is the photon energy.

[4] C. af Klinteberg (1999)

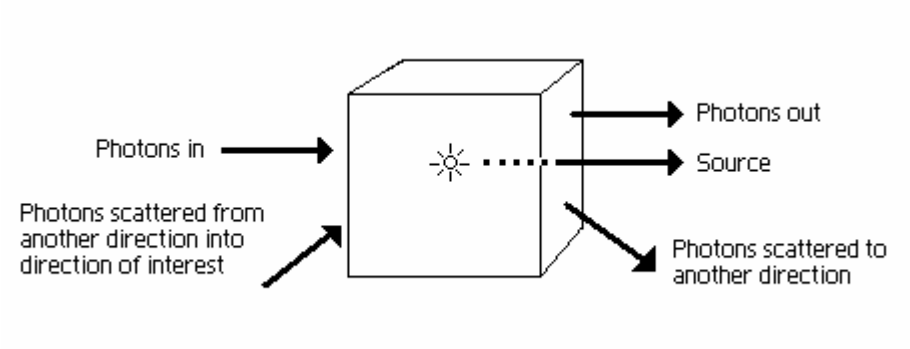

Figure 2.2. Schematic description of the different parts of the transport equation. (Figure adapted from M. S. Thompson[5]).

The five contributions are:

1. Transmitted light
2. Absorbed light
3. Light scattered out of the direction s
4. Light scattered into the direction s
5. Sources $Q(\bar{r},\bar{s}',t)$ within the volume

Together they give the time-dependent radiative transport equation.

$$\frac{1}{c}\frac{\partial L(\bar{r},\bar{s},t)}{\partial t} = -\underbrace{\bar{s}\cdot\nabla L(\bar{r},\bar{s},t)}_{1} - \underbrace{\mu_a L(\bar{r},\bar{s},t)}_{2} - \underbrace{\mu_s L(\bar{r},\bar{s},t)}_{3} + \underbrace{+\mu_s \int_{4\pi} L(\bar{r},\bar{s}',t)p(\bar{s},\bar{s}')d\omega'}_{4} + \underbrace{Q(\bar{r},\bar{s}',t)}_{5} \qquad (2.14)$$

Where μ_a is the absorption coefficient, μ_s the scattering coefficient, $p(\hat{s},\hat{s}')$ is the phase function describing the probability that light travelling in a direction $\hat{s}$ will be scattered into the direction $\hat{s}'$ and c the light velocity. $Q(\bar{r},\bar{s}',t)$ is the source term formed by the first scattering events of an incoming beam.

2.2.2 Solving the transport equation

The RTE has no analytical solution in three dimensions, but different numerical approaches can be applied. Different methods to obtain a solution are by using an expansion method such as the diffusion approximation, a discretisation method such as the adding-doubling method or a statistical method such as Monte Carlo simulations.[6] These three methods are described in the following sections.

[5] M. S. Thompson (2004)
[6] J. Swartling (2002)

2.2.3 The diffusion approximation

The diffusion approximation does not yield a full solution since it is an approximation. The basic idea is to expand the radiance L, the phase function p and the source term Q into spherical harmonics.

Expanding the radiance L in spherical harmonics results in

$$L(\bar{r},\bar{s},t)=\sum_{l=0}^{\infty}\sum_{m=-1}^{l}\sqrt{\frac{2l+1}{4\pi}}\psi_{lm}(\bar{r},t)Y_{lm}(\bar{s}) \tag{2.15}$$

Truncation of equation 2.15 at $l \geq 1$gives the P_1 approximation, which includes the 0^{th} and the 1^{st} terms but neglects terms of higher order.

$$L(\bar{r},\bar{s},t)=\sqrt{\frac{1}{4\pi}}\psi_{00}(\bar{r},t)Y_{00}+\sqrt{\frac{3}{4\pi}}\sum_{m=-1}^{1}\psi_{1m}(\bar{r},t)Y_{1m}(\bar{s})\approx$$
$$\approx\frac{1}{4\pi}\left(\phi(\bar{r},t)+3\bar{F}(\bar{r},t)\cdot s\right) \tag{2.16}$$

This equation should be interpreted as the radiance divided into one isotropic term Φ and one term F, which is the photon flux. They can be calculated using

$$\phi(\bar{r},t)=\int_{4\pi}L(\bar{r},\bar{s},t)d\omega \tag{2.17}$$

$$\bar{F}(\bar{r},t)=\int_{4\pi}L(\bar{r},\bar{s},t)\cdot\bar{s}d\omega \tag{2.18}$$

For an isotropic light source, the photon flux is given by Fick's law.

$$\bar{F}(\bar{r},t)=-D\nabla\phi \tag{2.19}$$

By expanding the source term Q in the same way, and the phase function p in a series of Legendre polynomials P_1, equations 2.20 and 2.21 will be obtained.

$$Q(\bar{r},\bar{s},t)=\frac{1}{4\pi}\left(q_0(\bar{r},t)+3q_1(\bar{r},t)\cdot s\right) \tag{2.20}$$

$$p(\bar{s},\bar{s}')=p(\cos\theta)=\frac{1}{4\pi}\sum_{l=0}^{L}(2l+1)b_1P_l(\cos\theta)\approx\frac{1}{4\pi}(1+3g\cos\theta) \tag{2.21}$$

In the case of an isotropic point light source, the term q_1 equals zero. By inserting equation 2.16, 2.20 and 2.21 into the transport equation 2.14, the time-dependent diffusion equation is obtained.

$$\frac{1}{c}\frac{\partial\phi(\bar{r},t)}{\partial t} = \nabla\big(D\nabla\phi(\bar{r},t)\big) - \mu_a(\bar{r})\phi(\bar{r},t) + q_0(\bar{r},t) \qquad (2.22)$$

D is the diffusion coefficient; c the speed of light in the medium, ϕ the light fluence rate and q_0 represents the light source. The conditions for which equation 2.22 is valid are that the light fluence rate must be calculated far away from the source and the absorption must be much smaller than the scattering, $\mu_a << \mu'_s$. The diffusion coefficient is defined as:

$$D = \frac{1}{3(\mu_a + \mu_s')} \qquad (2.23)$$

For steady state problems the time-independent diffusion equation is written as

$$-D\nabla^2\phi(\bar{r}) + \mu_a(\bar{r})\phi(\bar{r},t) = q_0(\bar{r},t) \qquad (2.24)$$

The solution to this equation is

$$\phi(\bar{r}) = \frac{P\mu_{eff}^2}{4\pi\mu_a}\frac{1}{|\bar{r}|}e^{-\mu_{eff}|\bar{r}|} \qquad (2.25)$$

Where P is the power of the incoming light and $\mu_{eff} = \sqrt{3\mu_a(\mu_a + \mu_s(1-g))}$.

To understand the solution to the equation applied to slab geometry, the case of a semi-infinite medium is first studied. Infinite means that no light escapes through the boundary of that surface and therefore the intensity at that surface can be set equal to zero.

Collimated beam, semi-infinite geometry
To simplify the problem, the assumption is made that all incident photons are initially scattered at the same depth z_0. Thus, z_0 corresponds to an isotropic source at the depth of one reduced scattering coefficient.

$$z_0 = \frac{1}{\mu_s'} \qquad (2.26)$$

When calculating the diffusion equation for anything but a homogeneous, infinite medium, boundary conditions must be fulfilled. One simple boundary condition is to set the fluence rate to zero at the boundary between the turbid and non-scattering medium. To solve this, mirror sources are introduced. Positive and negative sources are positioned above and below the boundary in such a way that the resulting fluence rate at the boundary is zero; se figure 2.3.

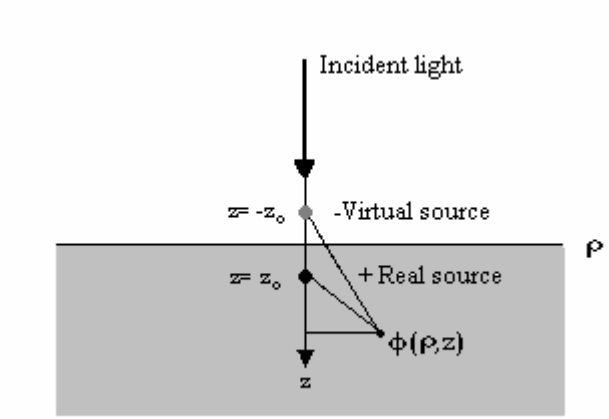

Figure 2.3. The principle of mirror sources. Mirror sources are introduced to get zero fluence rate at the boundary. The incident laser beam is modelled as an isotropic point source at a depth of z_0.

In reality there is always a Fresnel reflection in a boundary between media with different refractive indices, which results in a non-zero fluence rate at the physical boundary. One way to correct for this is to use the extrapolated-boundary condition, se figure 2.4, where the fluence rate is zero at a boundary located some distance outside the medium. This distance z_b is a function of the Fresnel reflection coefficient and z_0.

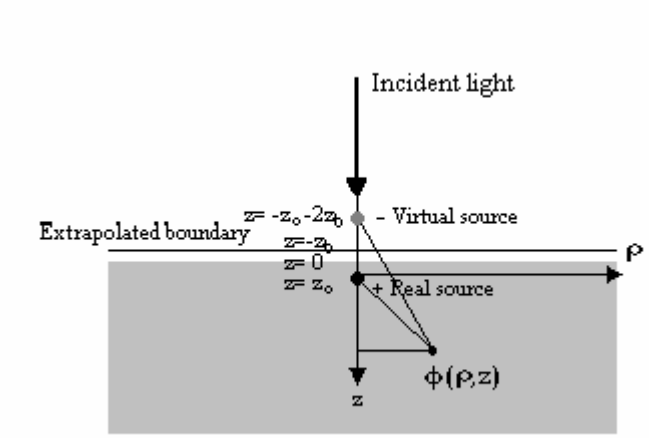

Figure 2.4. The extrapolated boundary principle. A collimated beam incident on a semi-infinite medium can be modelled as an isotropic point source at a depth z_0. A virtual negative source is mirrored in the plane $z= -z_b$ in such a way that the boundary conditions is fulfilled.

Collimated beam, slab geometry

With the slab geometry the boundary conditions gets more complicated to fulfil because now there are two surfaces to consider. A way to do this is to mirror the source in multiple planes. The source term in the diffusion equation is now a sum of positive and negative sources located above and below the slab. To get a good result, it might be necessary to mirror several times, see figure 2.5. For each mirroring the virtual sources are positioned further away from the slab and the contribution to the flux will decrease with this distance.[7]

[7] Andersson-Engels, Tissue Optics

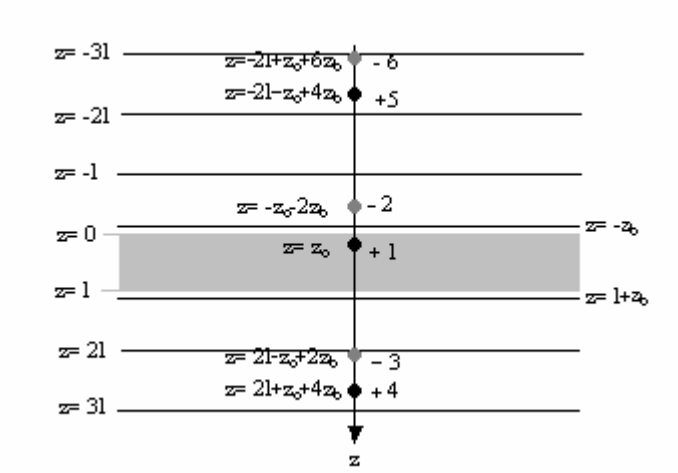

Figure 2.5. A collimated beam incident on a slab geometry. To be able to fulfil the boundary condition the source has to be mirrored several times. The source 1 is firstly mirrored in the plane $z= -z_b$, then both sources 1 and 2 are mirrored in the plane $z= l+z_b$ and sources 3 and 4 in the plane $z= -z_b$.

When the fluence rate is observed at a distance considerably larger than z_b the zero-radiance at the physical boundary is a valid approximation. At shorter distances, the extrapolated boundary is a better option. If the distance between source and detector is too short the diffusion approximation is not valid at all.[8]

For the case shown in figure 2.5, equation 2.25 will look like

$$\phi(\bar{r}) = \frac{P\mu_{eff}^2}{4\pi\mu_a}\left(\frac{1}{r_1}e^{-\mu_{eff}r_1} - \frac{1}{r_2}e^{-\mu_{eff}r_2} - \frac{1}{r_3}e^{-\mu_{eff}r_3} + \frac{1}{r_4}e^{-\mu_{eff}r_4} + \frac{1}{r_5}e^{-\mu_{eff}r_5} - \frac{1}{r_6}e^{-\mu_{eff}r_6}\right) \quad (2.27)$$

where $r_1, r_2,..,r_6$ are the distance to the respective source and are expressed by

$$r_1 = \sqrt{(z - z_0)^2 + \rho^2} \quad (2.28)$$

$$r_2 = \sqrt{(z + z_0 + 2z_b)^2 + \rho^2} \quad (2.29)$$

$$r_3 = \sqrt{(z - 2l + z_0 - 2z_b)^2 + \rho^2} \quad (2.30)$$

$$r_4 = \sqrt{(z - 2l - z_0 - 4z_b)^2 + \rho^2} \quad (2.31)$$

$$r_5 = \sqrt{(z + 2l - z_0 + 4z_b)^2 + \rho^2} \quad (2.32)$$

$$r_6 = \sqrt{(z + 2l + z_0 + 6z_b)^2 + \rho^2} \quad (2.33)$$

[8] S. Andersson-Engels, Tissue Optics

The transmittance, T, and the reflectance, R are found by

$$T(\rho) = hvJ(\rho,z)\cdot\bar{n} = -D\frac{\partial}{\partial z}\phi(\rho,z)\Big|_{z=d} =$$

$$= -\frac{1}{4\pi}\Bigg(-\frac{(d-z_0)}{r_1^2(z=d)}\left(\frac{1}{r_1(z=d)}+\mu_{eff}\right)e^{-\mu_{eff}r(z=d)_1} +$$

$$+\frac{(d+z_0+2z_b)}{r_2^2(z=d)}\left(\frac{1}{r_2(z=d)}+\mu_{eff}\right)e^{-\mu_{eff}r_2(z=d)} -$$

$$-\frac{(d-z_0+2z_b)}{r_3^2(z=d)}\left(\frac{1}{r_3(z=d)}+\mu_{eff}\right)e^{-\mu_{eff}r_3(z=d)} +$$

$$+\frac{(d+z_0+4z_b)}{r_4^2(z=d)}\left(\frac{1}{r_4(z=d)}+\mu_{eff}\right)e^{-\mu_{eff}r_4(z=d)} -$$

$$-\frac{(3d-z_0+4z_b)}{r_5^2(z=d)}\left(\frac{1}{r_5(z=d)}+\mu_{eff}\right)e^{-\mu_{eff}r_5(z=d)} +$$

$$+\frac{(3d+z_0+6z_b)}{r_6^2(z=d)}\left(\frac{1}{r_6(z=d)}+\mu_{eff}\right)e^{-\mu_{eff}r_6(z=d)}\Bigg) \quad (2.34)$$

$$R(\rho) = hvJ(\rho,z)\cdot\bar{n} = D\frac{\partial}{\partial z}\phi(\rho,z)\Big|_{z=0} =$$

$$= -\frac{1}{4\pi}\Bigg(-\frac{(-z_0)}{r_1^2(z=0)}\left(\frac{1}{r_1(z=0)}+\mu_{eff}\right)e^{-\mu_{eff}r(z=0)_1} +$$

$$+\frac{(z_0+2z_b)}{r_2^2(z=0)}\left(\frac{1}{r_2(z=0)}+\mu_{eff}\right)e^{-\mu_{eff}r_2(z=0)} -$$

$$-\frac{(2d-z_0+2z_b)}{r_3^2(z=0)}\left(\frac{1}{r_3(z=0)}+\mu_{eff}\right)e^{-\mu_{eff}r_3(z=0)} +$$

$$+\frac{(2d+z_0+4z_b)}{r_4^2(z=0)}\left(\frac{1}{r_4(z=0)}+\mu_{eff}\right)e^{-\mu_{eff}r_4(z=0)} -$$

$$-\frac{(2d-z_0+4z_b)}{r_5^2(z=0)}\left(\frac{1}{r_5(z=0)}+\mu_{eff}\right)e^{-\mu_{eff}r_5(z=0)} +$$

$$+\frac{(2d+z_0+6z_b)}{r_6^2(z=0)}\left(\frac{1}{r_6(z=0)}+\mu_{eff}\right)e^{-\mu_{eff}r_6(z=0)}\Bigg) \quad (2.35)$$

2.2.4 Inverse adding-doubling method

When the macroscopic parameters collimated transmittance, the total transmittance and the diffuse reflectance is known, the optical properties μ_a, μ_s and g can be obtained with the inverse adding-doubling method (IAD).

The adding-doubling method is a general, numerical solution of the radiative transport equation. The basic idea is to compare a slab with arbitrary thickness to a thin slab with known macroscopic parameters. By repeatedly doubling the thickness of the thin slab, the macroscopic parameters of the investigated slab may be found.[9]
The IAD method starts with a guess of the optical properties and solves the radiative transport equation using the adding-doubling method. The solution to this is then checked to the measured values. By repeatedly solving the radiative transfer equation until the solution matches the measured reflection and transmission values, the true optical properties of the sample are obtained. Inverse refers to the calculations that are done backwards; starting with the optical properties to get the transmittance and reflectance. The set of optical properties that gives a match with the measured reflection and transmission is taken as the optical properties of the sample[10].

The advantages of the IAD is that it provides accurate solutions for any combination of μ_a, μ_s and g as well as it handles the index mismatch between layers correctly. Drawbacks are that the method is restricted to layered geometries and uniform radiation. It doesn't readily give the light fluence inside the medium, each layer has to be homogeneous and the method is not time-resolved.[11] More information about the IAD-program can be found in the manual by S. A Prahl[12].

Optical properties
The IAD-program gives the albedo, the optical depth and the anisotropy factor g. These are dimensionless parameters that characterises light propagation, and from these parameters the scattering and absorption coefficient are easily obtained. The albedo *a* is defined as the ratio of scattering coefficient to the total attenuation coefficient.

$$a = \frac{\mu_s}{\mu_s + \mu_a} \tag{2.36}$$

The optical depth τ is the product of the sample thickness d and the total attenuation coefficient.

$$\tau = d\left(\mu_s + \mu_a\right) \tag{2.37}$$

[9] J. S. Dam (2000)
[10] S. A. Prahl et al (1993)
[11] J. Swartling (2002)
[12] S. A Prahl (1999)

The anisotropy factor g is the average cosine of the phase function as defined in equation 2.5.

The phase function used in this program is the Henyey-Greenstein phase function, see equation 2.38. This function is empirically chosen and gives results that coincide well with experimental work.

$$p(\cos\theta) = \frac{1}{4\pi}\frac{1-g^2}{\left(1+g^2-2g\cos\theta\right)^{3/2}} \qquad (2.38)$$

Input to the IAD-program is thickness and refractive index of the sample, information about how the experiment was carried out and finally the reflectance, R, transmittance, T, and collimated transmittance, T_{col}. The output is then the albedo, α, the optical depth, τ, and the anisotropy factor, g. If only R and T are known, the IAD-program will not give a value for g. Instead only the albedo and the optical depth are given, with the scattering coefficient, μ_s, replaced by the reduced scattering coefficient, μ_s'.

2.2.5 Monte Carlo method

This description of the Monte Carlo method basically follows the theory given in S.A Prahl's paper "A Monte Carlo Model of Light Propagation in Tissue"[13]. The Monte Carlo program uses a stochastic technique to simulate physical processes. Figure 2.6 shows the principles of the program and the theory behind each step will be briefly described in the following subsections.

Determining the step size Δs
A general rule when determining the step size Δs is that it should be much smaller than the reciprocal of the attenuation coefficient μ_t, see equation 2.39. However, this rule alone is not enough, because even if it is fulfilled it doesn't ensure an accurate result. If the step size is too small there will hardly be any interaction between photons and sample, but on the other hand, a step size that is too large will be a poor approximation to that of a real photon.

$$\Delta s << \frac{1}{\mu_t} = \frac{1}{\mu_s + \mu_a} \qquad (2.39)$$

A more efficient method is to determine different step sizes for each photon step. In this way, the program tries to equal the more realistic case where it is more probable for a photon to travel a short distance than a long, before a scattering or absorption event occurs. The probability density function, P, in equation 2.40 for Δs follows Beer- Lambert's law.

$$P \propto e^{-\mu_t \Delta s} \qquad (2.40)$$

[13] S. A Prahl et al (1989)

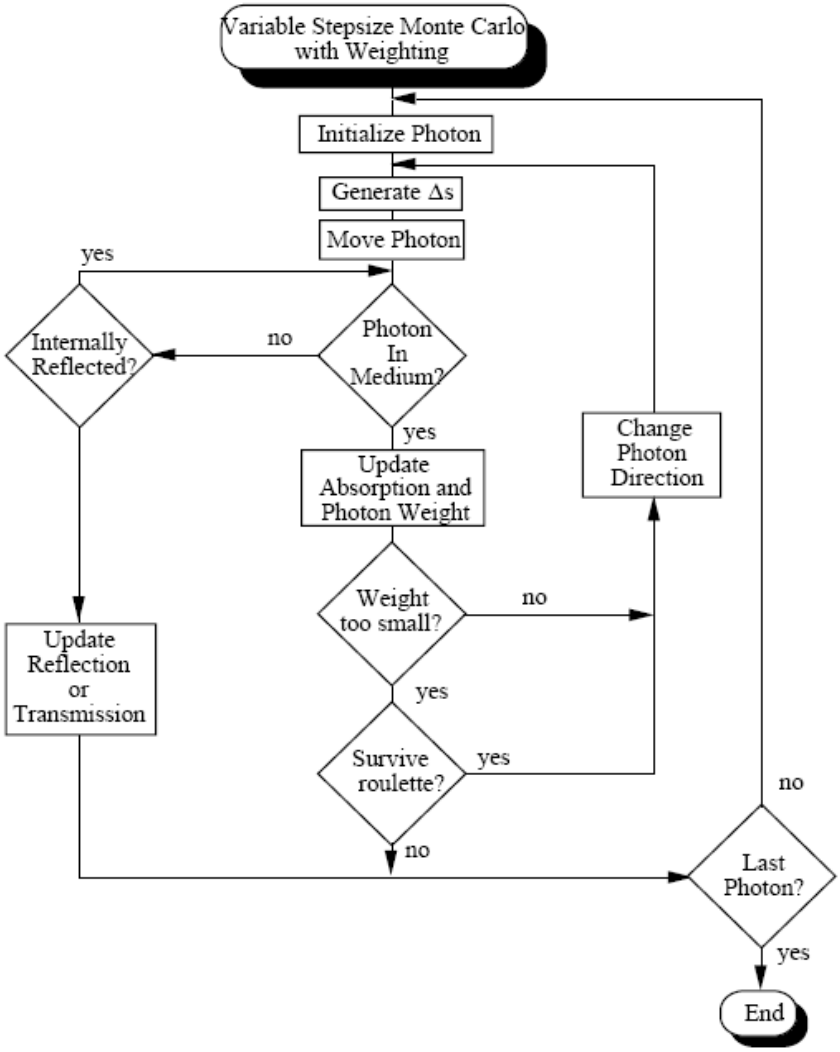

Figure 2.6. A flowchart showing the principles of the Monte Carlo Method. The photon is initialised and a step size generated after which the photon is moved. After that the photon can follow different paths and after each event the program is checking and updating absorption, photon weight and direction. Finally the photon weight is too small and the photon is either terminated in the roulette or given a new weight. [14]

To do this a function of a random variable ξ uniformly distributed between zero and unity is introduced. In this equation Δs represents the distance travelled by a photon before interacting with the sample by absorption or scattering.

$$\Delta s = \frac{-\ln \xi}{\mu_t} \tag{2.41}$$

Moving the photon

For the photon to be uniquely described five variables is necessary, three spatial coordinates for position and two directional angles for direction of travel. However, it is more convenient to use three Cartesian coordinates for the position, (x, y, z), and

[14] S. A Prahl et al (1989)

three direction cosines, (μ_x, μ_y, μ_z), for the direction of travel. Then the new position (x', y', z') of a photon after a scattering event is

$$x' = x + \mu_x \Delta s \tag{2.42}$$

$$y' = y + \mu_y \Delta s \tag{2.43}$$

$$z' = z + \mu_z \Delta s \tag{2.44}$$

Internal reflection
When the photon hits a boundary between two media with different refractive indices, it can be internally reflected. The reflection is determined by the Fresnel reflection coefficient, $R(\theta_i)$, equation 2.45. If a photon is being internally reflected or transmitted is decided by a random number ξ uniformly distributed between zero and unity. If $\xi < R(\theta_i)$ the photon is internally reflected, otherwise it is recorded to have left the sample.

$$R(\theta_i) = \frac{1}{2}\left[\frac{\tan^2(\theta_i - \theta_t)}{\tan^2(\theta_i + \theta_t)} + \frac{\sin^2(\theta_i - \theta_t)}{\sin^2(\theta_t + \theta_i)}\right] \tag{2.45}$$

The new photon position after it has been internally reflected, (x″, y″, z″) for a slab geometry is given by equation 2.46.

$$(x'', y'', z'') = \begin{cases} (x, y, -z) & , z < 0 \\ (x, y, 2\tau - z) & , z > \tau \end{cases} \tag{2.46}$$

The new photon direction (μ_x', μ_y', μ_z') is obtained by equation 2.47.

$$(\mu_x', \mu_y', \mu_z') = (\mu_x, \mu_y, -\mu_z) \tag{2.47}$$

Photon absorption
To determine if a photon is absorbed, the program uses a technique called implicit capture. Each photon packet is assigned a weight, ω, as it enters the sample. After each propagation step, the packet splits into two parts; the absorbed fraction and the scattered fraction. The absorbed fraction is expressed by equation 2.48.

$$\text{Absorbed fraction} = \frac{\mu_a}{\mu_s + \mu_a} = 1 - \frac{\mu_s}{\mu_s + \mu_a} = 1 - \alpha \tag{2.48}$$

Where α is the albedo mentioned in section 2.2.4. The new weight for the remaining, scattered part of the photon packet is then $w' = \alpha w$.

Photon termination
When the photon weight reaches a certain minimum, it is subject to a roulette that will decide the future of the photon. The photon of weight w gets a chance in m to survive with the new weight mw, or else its weight is reduced to zero.

Changing photon direction

When the photon direction is changed, the photon is scattered, there are two angles to be determined, the deflection angle, $\theta \in [0, \pi]$ and the azimuthal angle, $\varphi \in [0, 2\pi]$. If the scattering is isotropic the probability distribution for the cosine of the deflection angle is described by equation 2.49, where ξ is a random number between zero and unity.

$$\cos\theta = 2\xi - 1, \text{ if } g = 0 \tag{2.49}$$

Else it is described by the Henyey-Greenstein generating function in equation 2.50.

$$\cos\theta = \frac{1}{2g}\left\{1 + g^2 - \left[\frac{1-g^2}{1-g+2g\xi}\right]^2\right\}, \text{ if } g \neq 0 \tag{2.50}$$

The azimuthal angle is uniformly distributed between 0 and 2π.

$$\varphi = 2\pi\xi \tag{2.51}$$

For a photon that is scattered the angle (θ, φ) from the travelling direction (μ_x, μ_y, μ_z) the new direction (μ_x', μ_y', μ_z') can be calculated with equations 2.52-54.

$$\mu_x' = \frac{\sin\theta}{\sqrt{1-\mu_z^2}}\left(\mu_x\mu_z\cos\varphi - \mu_y\sin\varphi\right) + \mu_x\cos\theta \tag{2.52}$$

$$\mu_y' = \frac{\sin\theta}{\sqrt{1-\mu_z^2}}\left(\mu_y\mu_z\cos\varphi - \mu_x\sin\varphi\right) + \mu_y\cos\theta \tag{2.53}$$

$$\mu_z' = -\sin\theta\cos\varphi\sqrt{1-\mu_z^2} + \mu_z\cos\theta \tag{2.54}$$

If the angle is very close to normal, the following equations should be used to obtain the new direction.

$$\mu_x' = \sin\theta\cos\varphi \tag{2.55}$$

$$\mu_y' = \sin\theta\sin\varphi \tag{2.56}$$

$$\mu_z' = \frac{\mu_z}{|\mu_z|}\cos\varphi \tag{2.57}$$

2.3 Diode lasers

Diode lasers are a kind of semiconductor lasers that are found in many different applications in everyday life for example in CD players, laser printers and bar code readers. Other applications are medical diagnosis and treatment, optical memories and military systems. New applications are constantly emerging as new models appear with higher power, new wavelengths or lower costs.[15]

The performance of light emitting devices is based on the interaction of the electromagnetic light field with electronic excitations in the semiconductor. There are three different ways in which this interaction can occur, see figure 2.7 a; (1) absorption of light by an excitation of electrons from the valence band into the conduction band, (2) the inverse process, stimulated emission, where an incoming light quanta stimulates an electron to be de-excited from a state of higher energy into a state of lower energy, and (3) the spontaneous emission of light.[16] The principles of lasers are first to create a population inversion, that is more electrons in an excited state than in the ground state, se figure 2.7 a, and then to stimulate emission from the excited state. Spontaneous emission is unwanted because that reduces the population difference without the contribution of coherent photons.

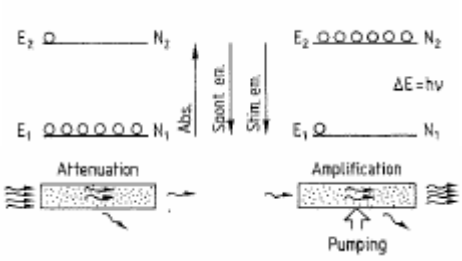

a. Different interaction processes. To create and keep a population inversion in a laser a pumping process is necessary.

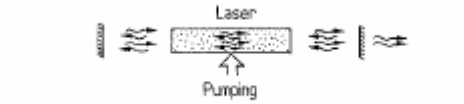

b. A laser consists of an active medium with the population inversion, a pumping process and a cavity which only lets out a small fraction of the photons.

Figure 2.7. Basic phenomena in laser action. The word Laser is an acronym for Light Amplification by Stimulated Emission of Radiation.[17]

Diode lasers consist of a doped semiconductor material. The population inversion exists in the transition zone between p- and n-doped materials and when a voltage is applied to the diode in the forward direction, laser action will take place, see figure 2.8 (b). The applied voltage is the pumping process in the diode laser, and it forces both electrons and holes into the transition region where the states in the conduction-band have excess population compared to the empty states in the valence-band. Laser

[15] Laser Physics
[16] H. Ibach and H. Lüth (2003)
[17] S. Svanberg (2004)

action with the photon energy corresponding to the band gap is obtained by recombination of electrons and holes.[18]

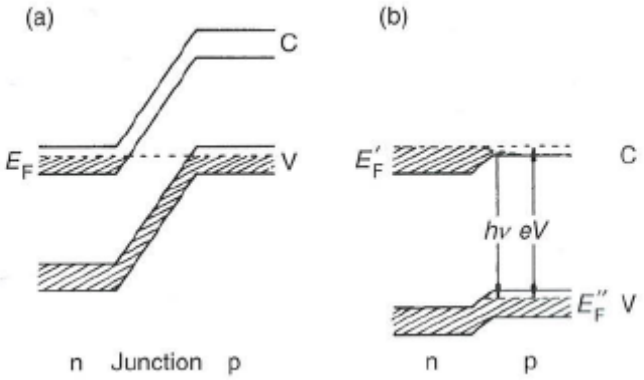

Figure 2.8. Energy levels in a diode laser. (a) The Fermi level E_F in the region of a p-n junction. (b) The result of applying a voltage across the junction; C is the conduction band and V the valence band.[19]

Diode lasers are some of the most efficient of all lasers, with an efficiency of about 30 per cent. Figure 2.9 shows a diode laser, the size is in the range of millimetres. Both ends are polished and form the laser cavity. Because of the geometry of the diode laser cavity, the beam is very divergent. This is a difference to most other kinds of lasers.[20]

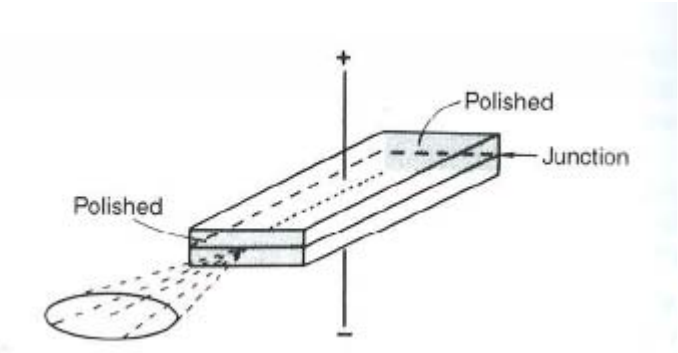

Figure 2.9. A diode, laser.[21]

[18] S. Svanberg (2004)
[19] J. M. Hollas (2004)
[20] J. M. Hollas (2004)
[21] J. M. Hollas (2004)

Chapter 3 Measurements and simulations

In this section the investigated samples are described, as well as the different experimental work and the simulations.

3.1 Description of samples

The material that has been tested is paperboard with different properties; table 1 gives a description of the different samples. The white surface of the thick samples has been coated with a substance that is reflecting in the visible range, and that also might effect the reflection in the infrared. The plastic coating is low density polyethylene, LDPE, which has the refractive index 1,51[22]. The refractive index of a cellulose fibre is 1,618 along the fibre, 1,544 in the transverse direction, determined for 590 nm[23]. Since most of the fibres are in the plane of the paper sheet, the transverse refractive index will be used.

To get all possible combinations, the paperboard is coated with LDPE on the white or brown side, or not at all for the two thicknesses. Measurements are done on both sides of each sample to see how the different surfaces and the white and brown paperboard layers affect the transmission. The samples are referred to by their number, and by adding a) for white side or b) for brown side facing the light source. The paperboard samples have two different thicknesses so that property will also be taken into account.

With the intention to investigate how an added substance affects the optical properties, the samples are also treated with mineral oil. The index of refraction for mineral oil is 1,469 for 589 nm[24], and decreases for longer wavelengths.

To calculate how much cellulose the paperboard consists of, pieces of sample 3 and 6 were weighted both untreated and prepared with oil. By knowing the density of mineral oil the ratio of volume fluid to volume paperboard could be calculated. The result was that paperboard consists of 40% air, and when treated with mineral oil this space is assumed to be filled by the oil. This is used when determining the refractive index of the treated and untreated paperboard, which is determined according to equation 3.1, where χ_i represent the volume fraction of material i with refractive index n_i.

$$n_{tot} = \chi_i n_i + \chi_j n_j \qquad (3.1)$$

The refractive indices used are n_{cell}= 1.54 for cellulose and n_{oil}= 1.46 for mineral oil.

[22] Plasticsusa
[23] M. Nogi (2005)
[24] NIST Standard Reference Materials Catalogue

Equation 3.1 yields the weighted refractive index n_{sample}^{*} = 1.324 for the samples (cellulose-air) n_{oil}^{*} = 1.51 for the samples treated with mineral oil (cellulose-mineral oil).

Table 3.1. A description of the different samples.

Sample	Side facing light	Thickness LDPE (µm)	Thickness paperboard (µm)	Weight paperboard (mg/cm2)	More
1	a) White b) Brown	40	270	17,8	LDPE on white
2	a) White b) Brown	40	270	17,8	LDPE on brown
3	a) White b) Brown	---	270	17,8	No LDPE
4	a) White b) Brown	40	440	28,5	LDPE on white
5	a) White b) Brown	40	440	28,5	LDPE on brown
6	a) White b) Brown	---	440	28,5	No LDPE

3.2 Integrating Sphere measurements

Using the integrating sphere, macroscopic parameters such as the reflectance and transmittance of a sample are measured. To get the optical properties from these measurements a theoretical model has to be applied. In this work, the Inverse adding-doubling model has been used for the evaluation followed by Monte Carlo simulations to verify the obtained optical properties.

3.2.1 Integrating Sphere theory and setup

In two different measurements, the integrating sphere setup measures the total diffuse light that has either been reflected or transmitted. A third measurement is required to be able to get all three optical parameters, μ_a, μ_s and g. This measurement gives the collimated transmission, from which the total attenuation coefficient, μ_t, can be evaluated; $\mu_t = \mu_a + \mu_s$.

The integrating sphere set up is shown in figure 3.1. Measurements are performed to obtain both the total and collimated transmittances as well as the diffuse reflectance. The set up consists of two optical arrangements. Firstly the integrating sphere, which has a diameter of 20 cm and the inside coated with highly reflecting barium sulphate. The sphere collects the total transmitted light flux through a sample when placed in position A and the diffusely reflected light flux when the sample is positioned at B. When the light has been transmitted or reflected by the sample, it is scattered multiple times inside the sphere and in that way transferred from being directed transmitted or reflected light to diffuse light fluxes. Now the light is independent of the direction and can be probed by an optical fibre bundle at one single position. The reflectance and transmittance can then be determined by equations 3.2 and 3.3.

$$R = R_{BS} \frac{I_R}{I_{ref}} \tag{3.2}$$

$$T = \frac{I_T}{I_{ref}} \tag{3.3}$$

I_R is the measured intensity of the reflectance flux (sample at position B), and I_T is the measured intensity of the transmittance flux (sample at position A and a barium sulphate plug at position B). The reference intensity, I_{ref}, is the measured intensity when the light flux is filling the sphere without interacting with any sample, only the barium sulphate plug at position B. The barium sulphate plug is a calibration standard with the reflectance factor, R_{BS}.

The second optical arrangement is used when measuring the collimated transmittance, which means that the light passes straight through the sample at position C with no light-sample interaction. The intensity, I_{col}, of the attenuated beam compared to the original intensity I_0 can then be expressed by equation 3.4.

$$I_{col} = \frac{I_0 \cdot e^{-(\mu_a+\mu_s)\cdot d}}{T_{ND}} \tag{3.4}$$

T_{ND} is the transmittance factor of the filters in front of the detection system. These filters are used during the reference measurement to prevent the detector from being saturated by the reference intensity which is much stronger than the intensity of the collimated transmittance. It is also preferable to have the two signals in the same intensity range to minimise non-linear effects caused by the detector.

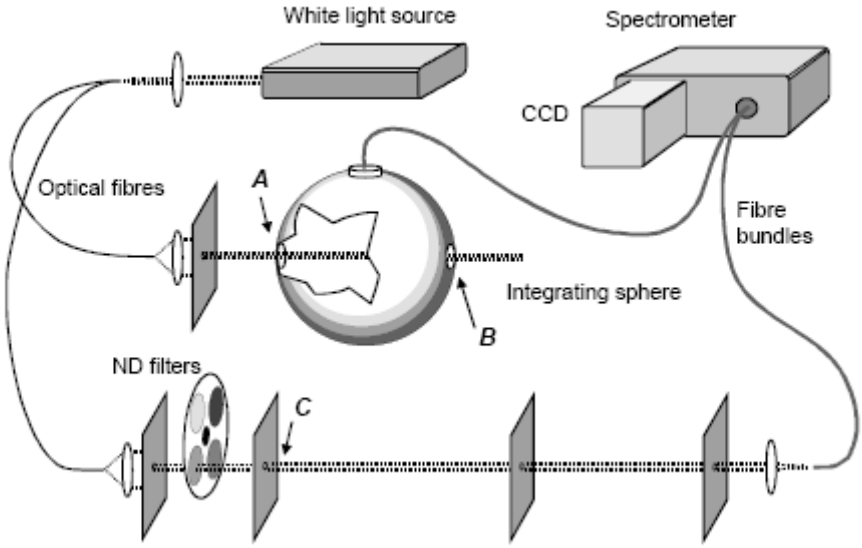

Figure 3.1. The integrating sphere set up. The transmittance is measured when the sample is in position A, the reflectance when the sample is in position B, and the collimated transmittance when the sample is in position C.[25]

The light source for both the optical arrangements is a 75W xenon lamp which generates white light. The light is guided by two optical fibres, one to the integrating sphere and the other to the collimated transmittance set up. To ensure that the light

[25] Tissue Optics

source is collimated and passes straight through the sample several lenses and aperture stops are inserted in the light path, as shown in figure 3.1. The probing light is then guided with two optical fibre bundles and the light from each bundle imaged separately on a spectrometer by two lenses. The detector used is a nitrogen-cooled CCD-detector.[26]

3.2.2 Experimental considerations

When doing the integrating sphere measurements, the samples where prepared in quadratic equal size pieces of 4x4 cm. The light spot size in the integrating sphere measurements was about 0.7 cm in diameter which is much larger than the inhomogeneity of the sample, but to get a reliable dataset measurements were done in three points on each sample. The results were then analysed both for the average and for the three points separately. A measurement was performed to determine the reflectance factor R_{BS}. This was done by comparing the reflection of the barium sulphate plug to the reflection of a known calibration standard.

3.3 IAD and Monte Carlo simulations

The input to the IAD-program are thickness and refractive index of the sample, information about how the experiment was carried out and finally the reflectance, R, transmittance, T, and collimated transmittance, T_{col}. The output is then the albedo, α, the optical depth, τ, and the anisotropy factor, g. If only R and T are known, the IAD-program will not give a value for g. Instead the output are the albedo and the optical depth, with the scattering coefficient, μ_s, replaced by the reduced scattering coefficient, μ_s'.

When performing the collimated transmittance measurement it is difficult to block all stray light, and that leads to uncertainties in the measured transmittance. The measured collimated transmittance might be higher than the actual transmittance and this will affect the optical parameters. Because of this, IAD-simulations were performed both with and without considering T_{col} and the results were compared.

Another problem was to decide which refractive index to use in the simulations. One option is to use the weighted refractive index of cellulose-air or cellulose-mineral oil, as described in section 3.1. Alternatively, the refractive index of the substance that fills the space between the cellulose fibres can be used. The motivation to this is that the photons are only scattered against the cellulose fibres, the photon propagation occurs in the space in between[27]. To bring clarity to what is the best option, both cases are simulated and the results compared.

When the refractive index is changed in the IAD-program this only affects the reflectance in the surfaces; the specular reflectance and internal reflection.

Now the optical properties have been determined by the IAD-program, and to verify the obtained coefficients they were inserted in the Monte Carlo program. The

[26] Tissue Optics
[27] J. R. Lorenzo (2000)

program used in this thesis is the MCML- Monte Carlo Simulation of Light Transport in Multi-layered Turbid media, version 1.2.2.[28]

In the MCML- program, the light is of the shape of a pencil beam. The input is the scattering and absorption coefficients, the anisotropy factor, refractive index and geometry information, and from that the reflectance and transmittance are calculated. By comparing these values to the values obtained from the IS-measurements the best set of coefficients is determined. These coefficients are the ones taken to describe the samples.

In the MCML program the samples are separated into two layers, the LDPE and the paperboard. The LDPE is assumed neither to absorb nor scatter any of the light. The only way the LDPE layer affects the simulation is with the surface reflection. By doing this separation of the layers, the simulation comes one step closer to describing the real samples.

To obtain a reasonable signal to noise ratio, 100 000 photon packets were launched in each simulation. Figures 3.2 and 3.3 show the signal and noise of the simulated transmittance. The noise is the difference between two simulations with identical input. The signal to noise ratio should be 10 or more, and this is fulfilled for the radius smaller than 0.8 cm, as shown in figure 3.4.

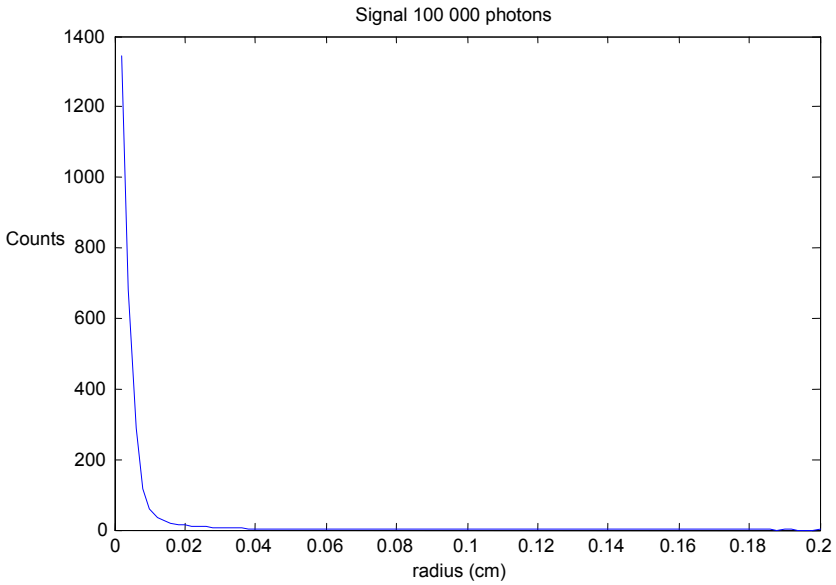

Figure 3.2 The transmission simulated with 100 000 photons.

[28] L.-H. Wang, S. L. Jacques, L, -Q. Zheng (1995)

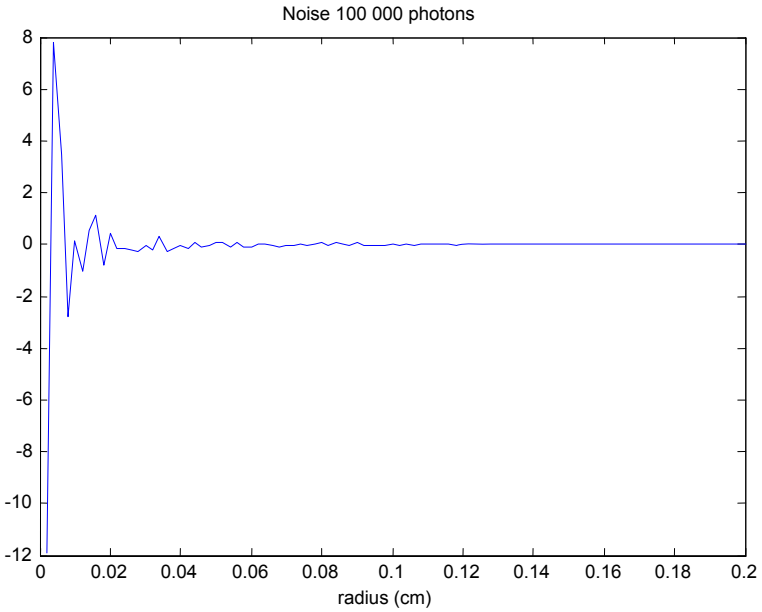

Figure 3.3 Noise in the simulations with 100 000 photons. This is the difference between two simulations with identical input parameters caused by the program.

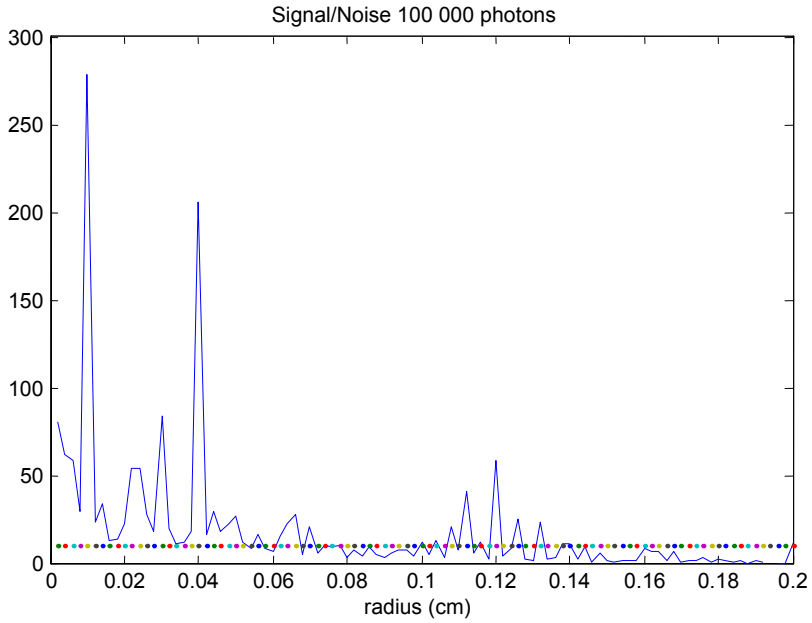

Figure 3.4 The signal to noise ratio of the obtained transmission. The ratio should be above 10 (the dotted line). This is obtained with a few exceptions for a radius smaller than 0.08 cm.

3.4 Tetra Pak Experiments

Experiments were done with the laser setup at Tetra Pak with the aim to relate these results to the results from the light propagation model.

3.4.1 Laser setup

The laser on Tetra Pak consists of four different diode lasers with specific wavelengths; 805, 850, 940 and 980 nm. Together they form a beam with a FWHM diameter of 0.31 cm and a maximum power of 200 W, each diode laser contributes

with a fourth of the power. The laser power is controlled by setting a pyrometer to a certain temperature, and then the laser power is regulated to give this temperature. The pyrometer measures the temperature in a small spot, much smaller than the laser spot size.

The laser beam is perpendicular to the samples, and measurements are done both when the samples are stationary and when they are passing the laser beam at a constant velocity.

3.4.2 Transmitted power

To measure the transmitted power, the samples are placed on a carbon black film. When the samples are illuminated by the laser, the carbon black absorbs all transmitted light and the temperature increases. A pyrometer set on a specific temperature is regulating the laser power so the carbon black holds the preset temperature.

By measuring the power required to heat the carbon black to 180°C both with and without a sample on top of the carbon black film, a value of the transmitted power is obtained. The measurements are performed on both sides of the samples and with the samples passing the laser beam with the velocity of 10 cm/s.

Chapter 4 Results and discussion

The purpose of the IS measurements followed by the IAD and Monte Carlo simulations was to determine the optical coefficients that describes the paperboard samples. These coefficients were then used in a model of the light propagation through the samples. Finally transmittance measurements at Tetra Pak was performed and compared with the results of the IS measurements and the light propagation model. In this chapter all results are presented and discussed.

4.1 Integrating Sphere measurements

From this measurement the total reflectance R, transmittance T and the collimated transmittance T_{col} were obtained. Since the samples are somewhat different, these values vary between the samples. Only the results for the wavelengths of the laser system at Tetra Pak: 805, 850, 940 and 980 nm are presented. The results are the averaged values from the three measurement points. Also the average of the four wavelengths is presented, as this will be compared to measurements on the Tetra Pak laser setup as well as the simulations.

Untreated samples
The results from the measurements are shown in table 4.1. From this it is apparent that the white side reflects more light, especially for the shorter wavelengths, and that the thinner samples have a higher transmittance. The LDPE-coating does not have an influence on the reflectance. The only property that affects the transmittance is the thickness; the thick samples transmit 45 % compared to the thin samples. The lower reflectance of the brown side does not give a higher transmittance which indicates that the difference in reflection depends on absorption in the brown surface. At 805 nm the difference is about seven and thirteen percentage points for the thin and thick samples respectively.

Table 4.1. Reflectance and transmittance of the untreated samples. First value represents the reflectance and the second the transmittance. The last column represent the average reflectance and transmittance of the four wavelengths. The LDPE in the "Side facing light" column indicates the surfaces with LDPE coating. Samples 1-3 have the thickness 0.03 cm and samples 4-6 has the thickness 0.05 cm.

Sample	Side facing light	R+T (%)	R+T (%)	R+T (%)	R+T (%)	Average R+T (%)
	Wavelength (nm)	805	850	940	980	
1	a) White LDPE	79+ 14	80+ 15	80+ 17	81+ 17	80+ 16
	b) Brown	73+ 14	75+ 16	79+ 17	80+ 17	77+ 16
2	a) White	80+ 14	80+ 15	81+ 17	81+ 17	81+ 16
	b) Brown LDPE	72+ 14	75+ 15	78+ 17	79+ 17	76+ 16
3	a) White	81+ 13	82+ 14	83+ 16	83+ 17	82+ 15
	b) Brown	73+ 13	76+ 15	79+ 17	80+ 17	77+ 16
4	a) White LDPE	86+ 6	86+ 7	87+ 9	87+ 9	87+ 8
	b) Brown	73+ 6	77+ 8	81+ 9	82+ 10	78+ 8
5	a) White	85+ 6	86+ 8	86+ 9	87+ 10	86+ 8
	b) Brown LDPE	73+ 7	77+ 9	81+ 11	83+ 11	79+ 10
6	a) White	84+ 6	85+ 7	86+ 9	86+ 9	85+ 8
	b) Brown	71+ 7	75+ 8	81+ 10	82+ 11	77+ 9

Samples treated with mineral oil

Adding mineral oil to the samples resulted in a considerable increase in transmittance (and decrease in reflectance), as seen in table 4.2. The difference in transmittance between the two thicknesses is smaller as the thick samples transmit about 87 % compared to the thin samples. The difference in reflection between the brown and white side have decreased compared to the untreated samples, it is only one or a few percentage points but it is noticeable in the transmittance as well. This indicates that the difference in reflectance has not been absorbed, but transmitted, and that the oil facilitates light propagation through both surfaces and the bulk material.

Table 4.2. Reflectance and transmittance of the samples treated with mineral oil. First value represents the reflectance and the second the transmittance. The last column represent the average reflectance and transmittance of the four wavelengths. The LDPE in the "Side facing light" column indicates the surfaces with LDPE coating. Samples 1-3 have the thickness 0.03 cm and samples 4-6 has the thickness 0.05 cm.

Sample	Side facing light	R+T	R+T	R+T	R+T	Average R+T
Oil	Wavelength (nm)	805	850	940	980	
1	a) White LDPE	35+ 57	36+ 60	36+ 62	36+ 63	36+ 61
	b) Brown	34+ 59	35+ 61	34+ 63	34+ 65	34+ 62
2	a) White	35+ 58	36+ 61	35+ 63	35+ 64	35+ 62
	b) Brown LDPE	34+ 57	35+ 60	35+ 62	35+ 64	35+ 61
3	a) White	32+ 62	32+ 64	32+ 67	32+ 68	32+ 65
	b) Brown	31+ 61	31+ 63	31+ 66	31+ 68	31+ 65
4	a) White LDPE	39+ 49	41+ 53	41+ 56	41+ 56	41+ 53
	b) Brown	37+ 52	39+ 55	39+ 57	40+ 58	39+ 55
5	a) White	39+50	40+ 53	41+ 56	41+ 57	40+ 54
	b) Brown LDPE	37+ 52	38+ 54	40+ 57	40+ 59	39+ 56
6	a) White	40+ 50	41+ 53	41+ 56	41+ 57	41+ 54
	b) Brown	36+ 53	37+ 56	38+ 58	39+ 59	38+ 57

Comparison between untreated and treated samples

At 805 nm, the transmittance of the untreated samples is approximately 23% and 13% of the transmittance of the treated samples, for the thin and thick samples, respectively. At 980 nm, the same comparison gives 26% for the thin samples and 17% for the thick samples.

The reflectance is also considerably lower for the treated samples, about half compared to the untreated for all wavelengths.

Reflectance can be divided into two parts. Part one is the specular reflection at the surface that is depending on the difference in refractive index and which can not be avoided. Part two is the light that has penetrated the surface but is backscattered inside the material and leaves the material on the same side as it came in. This is the part that can be reduced by treating the paperboard with a suitable medium. The important properties of such a medium are a refractive index that is close to that of the paperboard, that is, cellulose, and to obtain maximum transmittance, no or very low absorption.

Part one of the reflectance, the specular reflection can be affected by treating the surface, in this case with the LDPE coating, but the IS measurements show that the LDPE does not result in a positive impact on either reflectance or transmittance. Regarding the refractive index of the LDPE layer, it is rather close to that of cellulose

as is desired. But since it is only a layer on the surface of the paperboard it keeps the light from propagating in the same way as the cellulose fibres do.

By comparing the transmittance of a sample that has been favourably treated on the surface; an untreated sample with the LDPE coating, with a sample that has been treated throughout the sample; a sample treated with mineral oil, it is evident that it is the diffuse reflectance that is different between the two. The specular reflectance is almost the same since the refractive index of LDPE is 1.50 and mineral oil 1.46. To increase the transmission the sample must be made more homogeneous in terms of refractive index variations. It is not enough only to change the surface properties.

4.2 Inverse Adding-doubling simulations

The IAD-program evaluates the optical coefficients of a sample given the reflectance and transmittance of that sample. The coefficients are the absorption coefficient, μ_a, the scattering coefficient μ_s, and the anisotropy factor, g.

In this section the coefficients are presented; evaluated with the IAD-program with transmittance and reflectance data from the IS measurements. The coefficients are only presented for the wavelengths 805, 850, 940 and 980 nm.

It is important to keep in mind that the IAD-program assumes that the sample is homogeneous. In reality the samples consists of two layers of paperboard, one brown and one white. In addition to this there is a layer of LDPE on some of the samples that is not taken into account in the IAD-program. This means that the obtained coefficients can be considered as the best approximation possible.

The samples were studied from both sides to form an opinion of how the layered structure impacts the evaluated coefficients, and to get an idea of how much of a problem the layered structure pose.

4.2.1 R, T versus R, T, T_{col}

It is difficult to measure the collimated transmittance and because of this the IAD-simulation based on all three parameters R, T and T_{col} includes uncertainties. Simulations based on only R and T are assumed to give more reliable results, though it involves not being able to determine the anisotropy factor and the scattering coefficient separately. Instead the reduced scattering coefficient is obtained together with the absorption coefficient.

The comparison of the IAD simulation based on R,T and T_{col} with the one based on only R and T were performed with the purpose to see if the collimated transmittance had been measured properly. If it has, there will be no difference between the evaluated coefficients, and the sample can be described with all three coefficients; μ_a, μ_s and g. If there is a difference, the coefficients evaluated from the R and T simulation are a better choice.

When comparing the IAD-results from R, T and R, T, T_{col} the weighted refractive index was used.

Untreated samples

The R, T, T_{col}-and the R, T-simulation gave close to identical coefficients for the thinner samples 1, 2 and 3, both absorption and reduced scattering coefficients. The evaluated coefficients of sample 1 are shown in figures 4.1 and 4.2, and the results of sample 2 and 3 are similar. Regarding the thicker samples, 4, 5 and 6 there was a difference in the evaluated coefficients when the white side was facing the light, side a. Figures 4.3 and 4.4 show the evaluated coefficients for sample 6, the difference between the coefficients for the a-side decreases as with longer wavelength.

It is interesting to note that the evaluated reduced scattering coefficient depends differently on the wavelength for the different sides, for white or brown side facing the light, and that the scattering coefficient is much larger when the white side is facing the light source.

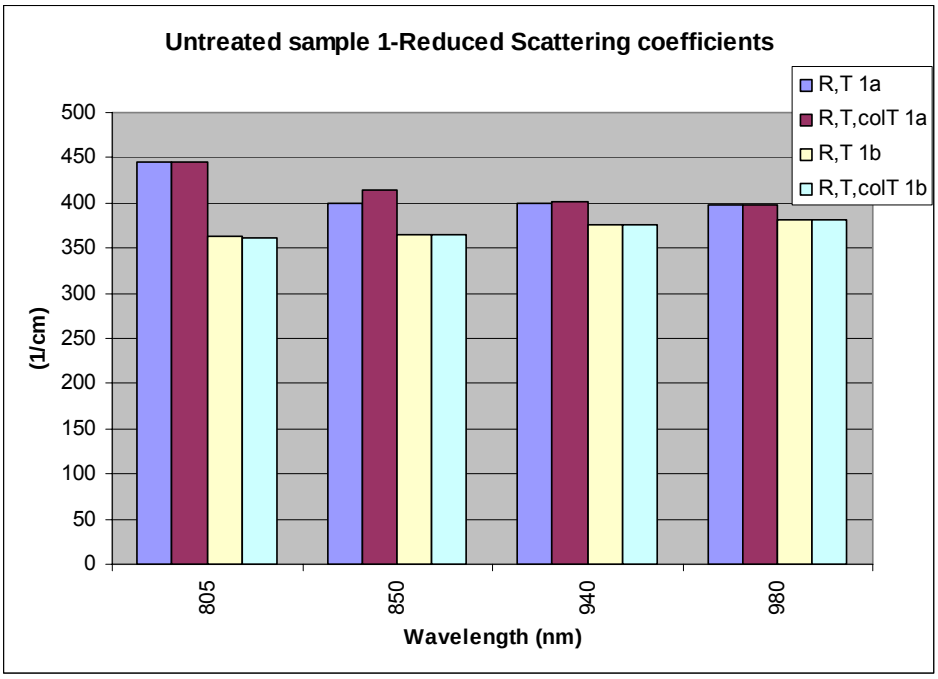

Figure 4.1 Reduced scattering coefficients μ_s' of the untreated sample 1 when using R and T in the IAD-simulation compared to when using R, T and T_{col}. Both simulations gave almost identical coefficients for both white and brown side facing the light.

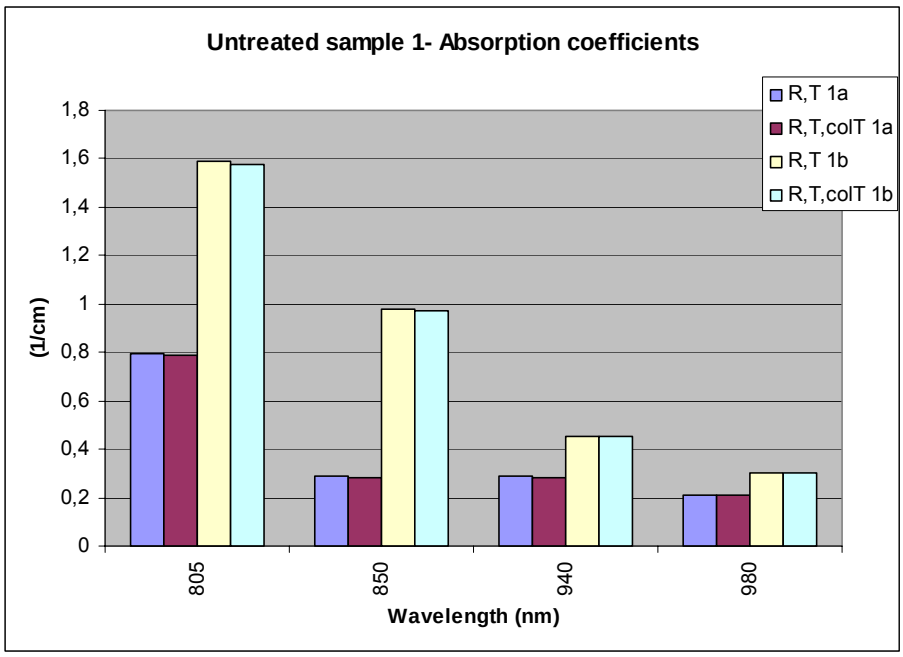

Figure 4.2 The absorption coefficients μ_a of the untreated sample 1 when using R and T in the IAD-simulation compared to when using R, T and T_{col}. Both simulations gave identical coefficients for both white and brown side facing the light.

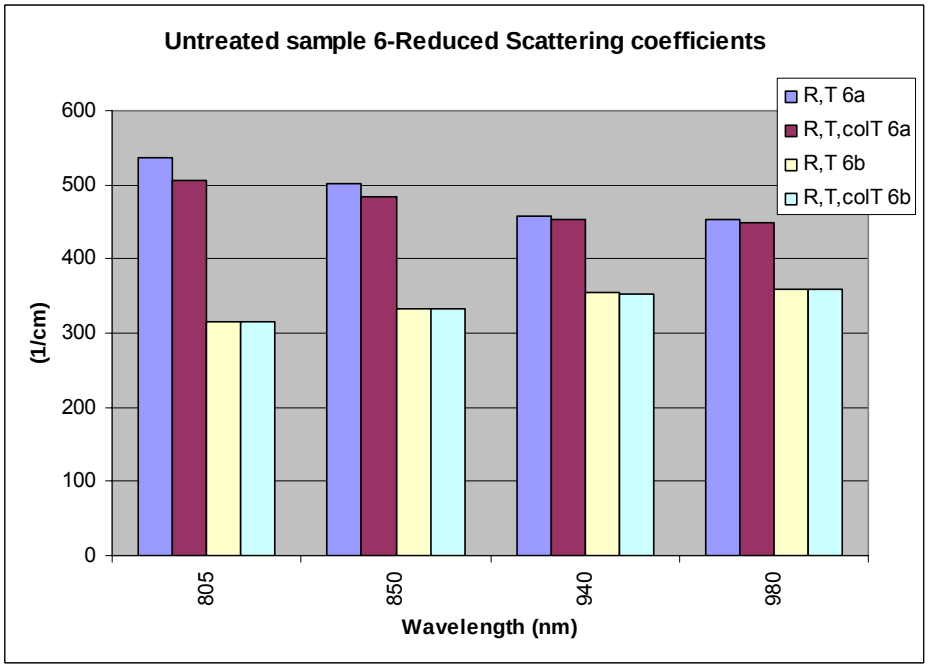

Figure 4.3 The reduced scattering coefficients μ_s' of the untreated sample 6 when using R and T in the IAD-simulation compared to when using R, T and T_{col}. The difference in the evaluated reduced scattering coefficients are more evident at the two shorter wavelengths.

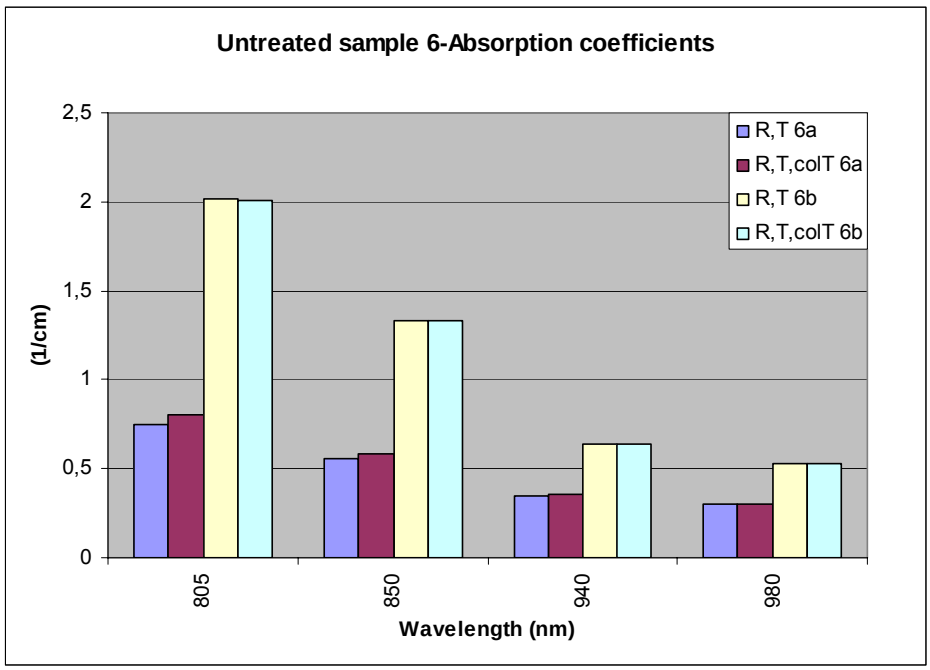

Figure 4.4 The absorption coefficients μ_a of the untreated sample 6 when using R and T in the IAD-simulation compared to when using R, T and T_{col}. There is a small difference in absorption coefficients between the two simulations for the wavelengths 805 and 850 nm, when the white side is facing the light.

Samples treated with mineral oil

The simulations on the samples treated with mineral oil did not show the same uniformity as the untreated samples. For all samples, the simulation using R and T gave a higher reduced scattering coefficient than the simulation with R, T and T_{col}. Compared to the untreated samples, the difference in reduced scattering coefficient between the a- and b side is much smaller. The obtained absorption coefficients from the two simulations correlate very well. The coefficients of samples 1, thickness 0.03 cm, and 6, thickness 0.05 cm, are presented in figures 4.5 to 4.8.

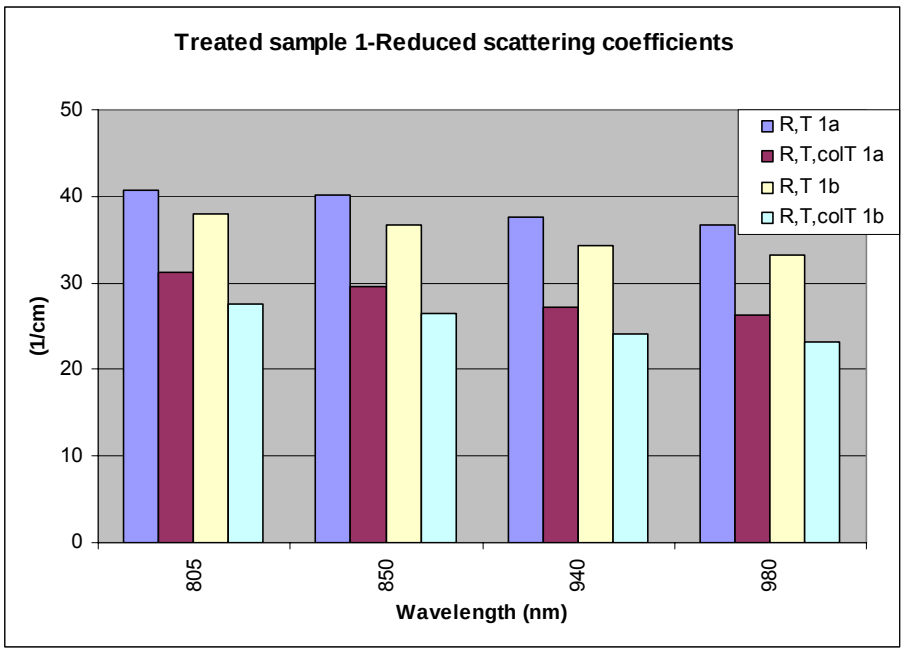

Figure 4.5 The reduced scattering coefficients μ_s' of the treated sample 1 when using R and T in the IAD-simulation compared to when using R, T and T_{col}. The two simulations result in a rather big difference between the evaluated coefficients, the R,T simulation gives a higher value for both sides.

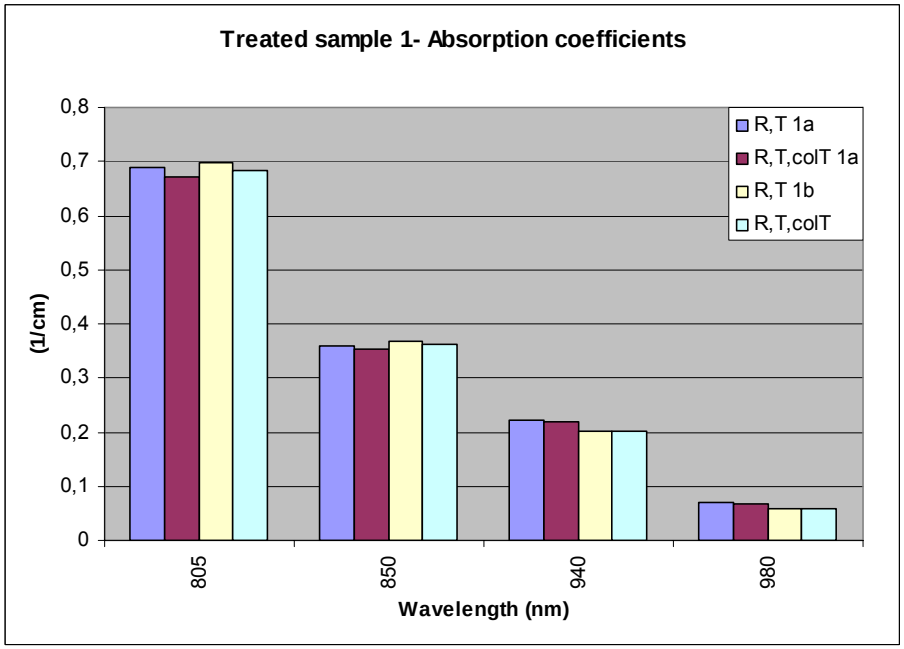

Figure 4.6 The absorption coefficients μ_a of the treated sample 1 when using R and T in the IAD-simulation compared to when using R, T and T_{col}. The two simulations give almost identical absorption coefficients for both white and brown side facing the light.

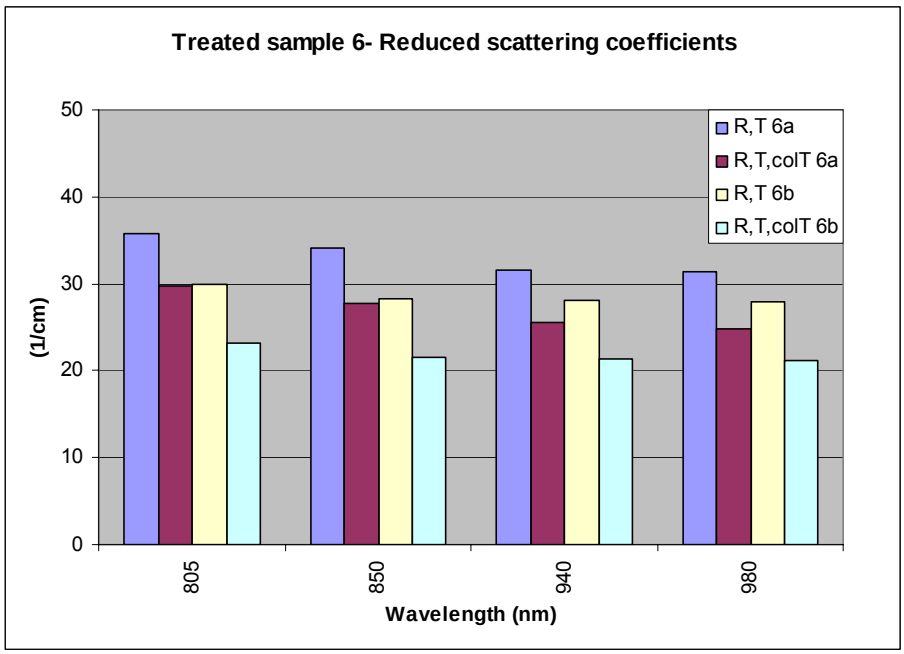

Figure 4.7 The reduced scattering coefficients μ_s' of the treated sample 6 when using R and T in the IAD-simulation compared to when using R, T and T_{col}. The R, T simulation results in higher coefficients for both sides.

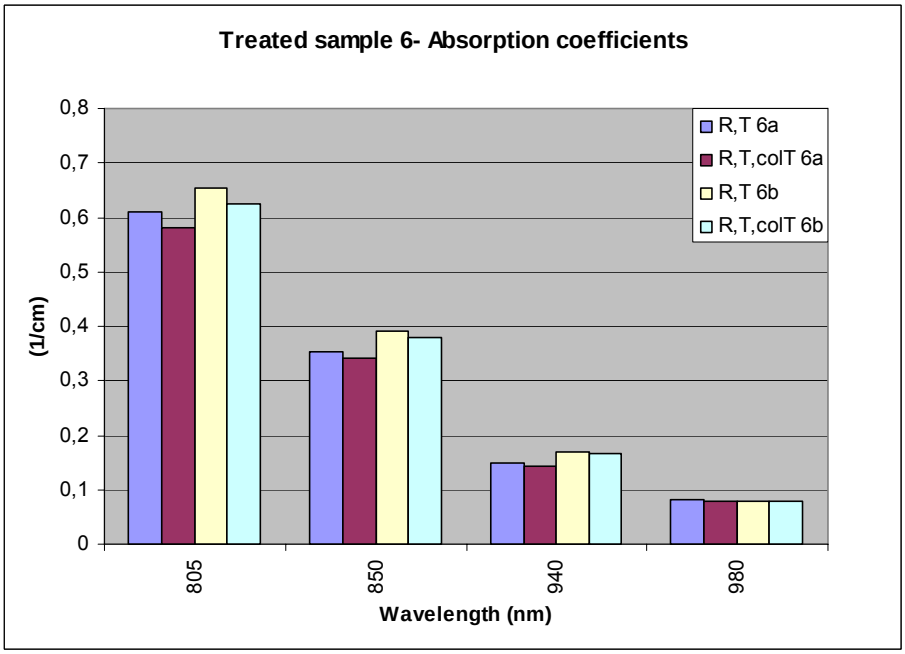

Figure 4.8 The absorption coefficients μ_a of the treated sample 6 when using R and T in the IAD-simulation compared to when using R, T and T_{col}. There is a small difference for the two shorter wavelengths.

4.2.2 Weighted versus air/ mineral oil refractive index

Paperboard consists of cellulose but also a rather large part air, causing a problem when choosing which refractive index to use in the simulations. One option was to use the weighted refractive index of cellulose-air or cellulose-mineral oil, as described in section 3.1. Alternatively, the refractive index of the substance that fills the space between the cellulose fibres can be used, with the motivation that the

photons are only scattered against the cellulose fibres, the photon propagation occurs in the space in between[29].

By changing the refractive index in the IAD simulations, only the specular reflections in the surfaces is changed, as well as the internal reflection. This will not totally account for the impact a change in refractive index would pose in reality.

Untreated samples
The following figures show scattering and reduced scattering coefficient as well as the absorption coefficients of samples 5 a with weighted refractive index n= 1,324, compared to the refractive index for air n= 1,0.

The scattering coefficient of all samples show a good agreement between the two simulations, but in the reduced scattering coefficient there are differences. The a-side of the thick samples 4, 5 and 6 show a strange result, sample 5a is presented in figure 4.9. The reduced scattering coefficient for n= 1.0 alters rather quickly between a high value for 805 nm to a low value for 850 nm and then it stabilises. This difference is not fully understood, or if it is resulting as a problem from the measurements. If correctly measured, it should be the g-factor that is responsible for this since the scattering coefficients are the same.

Figure 4.10 show the absorption coefficient of sample 5a. For most cases the n=1.0 simulation gives a higher absorption.

Since the simulation with n= 1.0 gives no specular reflection in the surfaces or internal reflection in the end surface, as well as a peculiar g-factor for the thicker samples, the simulation with the weighted refractive index is the better choice.

[29] J. R. Lorenzo (2000)

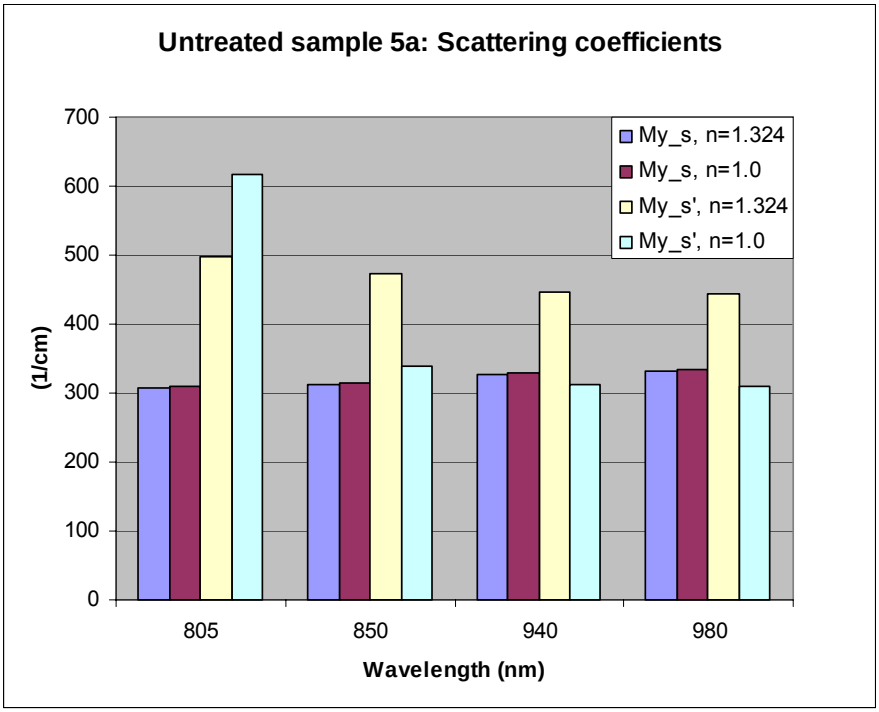

Figure 4.9 Scattering and reduced scattering coefficients of sample 5a obtained by IAD-simulations with two different refractive indices. The simulation with n=1.0 shows a peculiar leap in the reduced scattering coefficient, n=1.0, from a high value at 805 nm to a low at 850 nm.

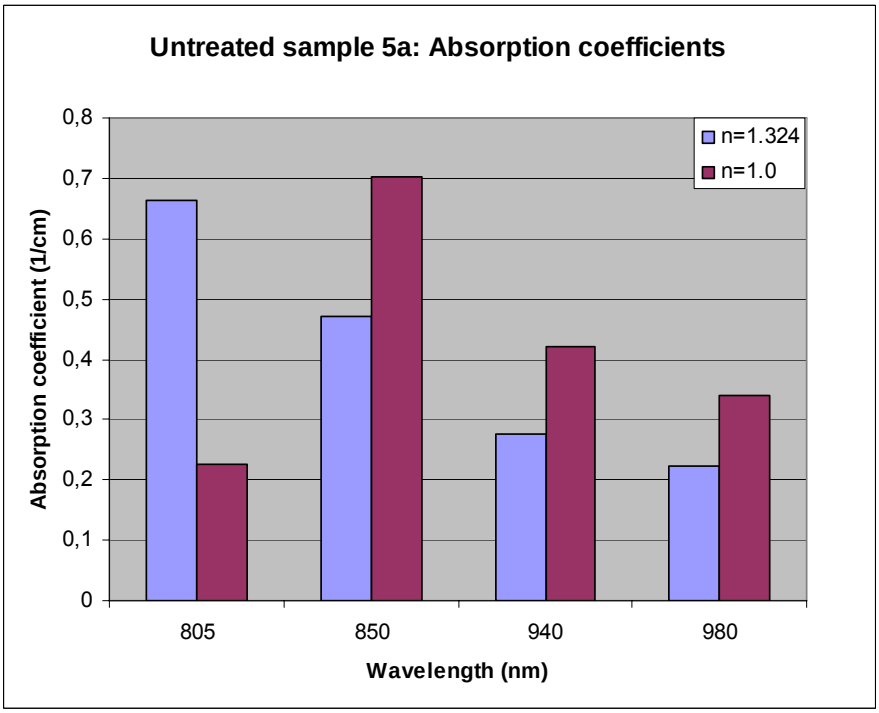

Figure 4.10 Absorption coefficients of sample 5a obtained by IAD-simulations with two different refractive indices.

Samples treated with mineral oil

The two simulations with the treated samples gave almost identical coefficients; the difference between the refractive indices is too small to have an impact.

4.2.3 Differences between the samples- Weighted refractive index

The following figures show a comparison of the evaluated reduced scattering coefficient of the thin and thick samples, respectively.

Because of the difficulties with measuring the collimated transmittance T_{col}, the simulation based on all three parameters R, T and T_{col} will include greater uncertainties than the simulation based on only R and T. On account of this, the following results are from the IAD-simulation with only R and T as inputs.

Untreated samples
There is a distinct difference between the coefficients obtained from the white or brown side, especially regarding the thicker samples. The difference between the maximum and minimum reduced scattering coefficient is 40 % for the thick samples and 30 % for the thin at 805 nm. The difference decreases with increasing wavelength giving a difference of 21 % for the thick samples and 17 % for the thin at 980 nm.

The thickness impact the scattering coefficients, the thicker samples have a bigger difference between the scattering coefficients obtained from the different sides, than the thin. This might be because the thick samples have the reflective coating which the thin have not. The brown side yields a lower scattering coefficient that could result from more absorption because the thickness of the brown layer is bigger than the thickness of the white.

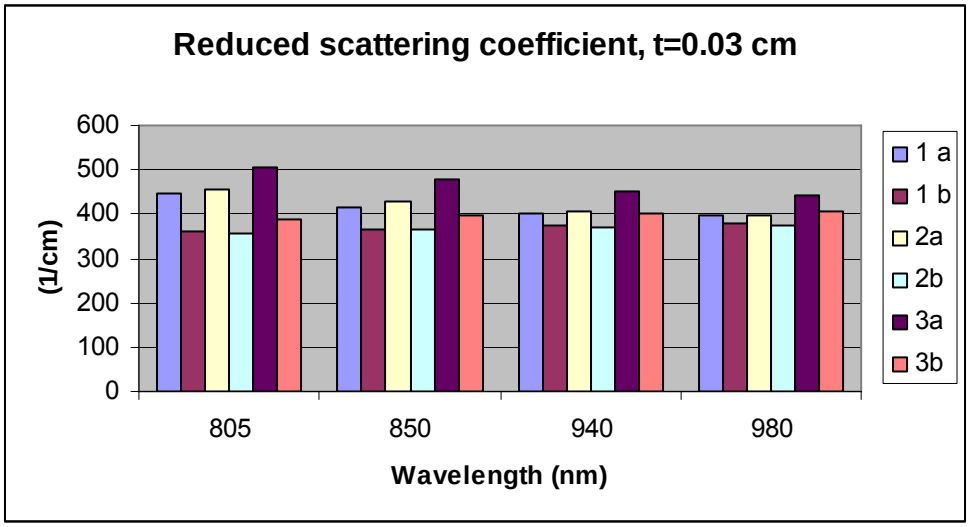

Figure 4.11. The reduced scattering coefficients of the untreated samples with thickness t=0.03 cm, a represents white and and b brown side facing the light. The differences between the two sides decrease with increasing wavelength.

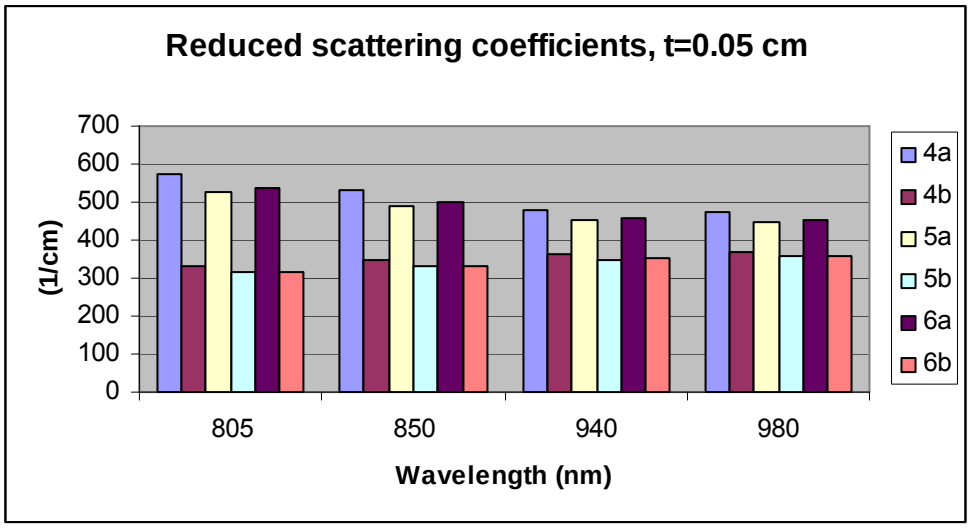

Figure 4.12. The reduced scattering coefficients of the untreated samples with thickness t=0.05 cm. There is a separation between the a- and b sides, and the evaluated coefficients depend differently on the wavelength.

Samples treated with mineral oil

Adding oil to the samples resulted in a significantly lower reduced scattering coefficient, about 10 times smaller. The differences between a- and b sides of the thicker samples are no longer that large, about 14%, at 805 nm and 15% at 980 nm. Regarding the thin samples there are no longer an evident difference depending on the different sides. The absorption coefficient of the brown sides has decreased to a level corresponding to the lower absorption coefficients obtained from the white, untreated side. The thinner samples have a higher scattering coefficient that could depend on reflections in the surfaces. These reflections exists equally much in both thicknesses, but the impact on the scattering coefficient, that is expressed in cm^{-1}, of the thin samples is bigger because the distance between the surfaces is shorter.

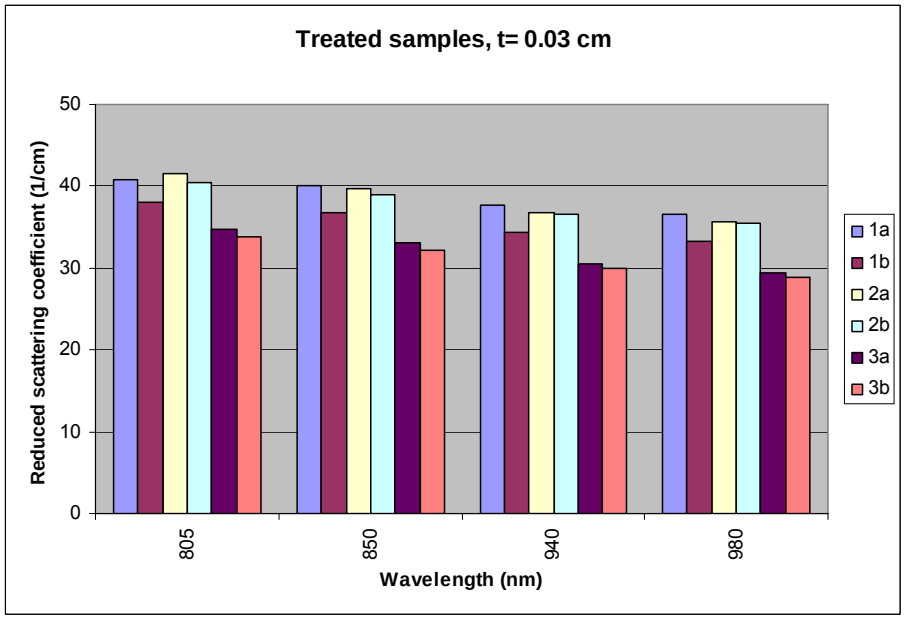

Figure 4.13 The reduced scattering coefficients of the treated samples with thickness t=0.03 cm. The oil has reduced the difference between the coefficients of the two sides and now the evaluated coefficients show the same wavelength dependency.

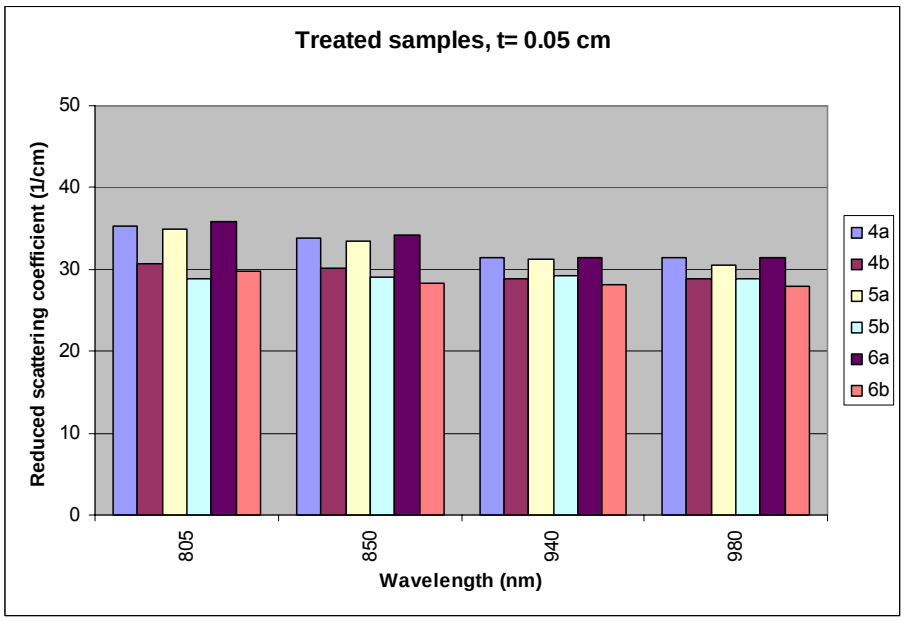

Figure 4.14 The reduced scattering coefficients of the treated samples with thickness t=0.05 cm show a slight separation between the sides.

Summary of the IAD results

Since the samples are made of the same material the coefficients of the bulk material are supposed to be the same. The differences arise from the fact that the surface properties influence the measured results in a way that is not accounted for in the simulations in the case of the untreated samples. A white surface yields a higher scattering coefficient than a brown because of more reflection at the surface which results in an overestimation of the scattering inside the sample. This also affects the g-factor that is assigned a negative value; the scattering is assumed to be directed backwards. When the brown side is facing the light source more light is enering the bulk of the material and is thereby given a higher probability to get absorbed and a lower scattering coefficient is also resulting in the evaluation.

The evaluated absorption coefficient is much lower than the scattering coefficient, which is not surprising since cellulose is chains of sugar molecules $(C_6H_{10}O_5)_n$. The different bonds in the cellulose molecule are between O-H and C-O. These bonds both have absorption features at wavelengths longer than 2.8 μm and do not affect the region of interest.[30] Adding oil to the samples results in lower absorption coefficients for both sides, similar to those obtained from the white, untreated side.

Regarding the transmission, it doesn't matter if it is the brown or the white side that is facing the light source. There is a difference in reflectance but that is not of interest for the application at Tetra Pak. From the IS measurements it is clear that the surface properties do not affect the transmission and which ever of the coefficient sets chosen will represent the transmission correctly.

Investigating the samples closer, they consist of a larger part brown paperboard and therefore it seems most reasonable to choose the coefficients resulting from the case where the brown side is facing the laser. The difference in reflectance might later be

[30] C. N. Banwell, E. M. McCash (1994)

corrected by the knowledge that the brown side absorbs and the white side reflects more of the light. The resulting coefficients from the brown side are considered more accurate in terms of describing the bulk material.

To summarize the IAD-results the mean values and standard deviations of the coefficients are presented in table 4.3; the mean values are chosen as the coefficients that describe the samples. Regarding the untreated samples only the results from the b-sides are considered as discussed above. Since the simulations of the treated samples do not result in that big differences in the coefficients between the samples, both sides are considered when choosing the final set of coefficients.

Table 4.3. The mean and standard deviation of the reduced scattering and absorption coefficient for the four wavelengths.

	Wavelength (nm)	805	850	940	980
Untreated (Only b-sides)	μ_s' (1/cm)	345,1± 27,4	355,7±23,3	368,8±18,8	375,1±17,2
	μ_a (1/cm)	1,75± 0,40	1,13± 0,26	0,54± 0,12	0,40± 0,11
Treated	μ_s' (1/cm)	35,4± 4,4	34,1± 4,1	32,2± 3,4	31,5± 3,1
	μ_a (1/cm)	0,69± 0,08	0,38± 0,07	0,19± 0,06	0,07± 0,05

4.3 Monte Carlo simulations

When the optical parameters of a sample are known, a Monte Carlo program can be used to simulate the reflectance and transmittance of the sample. In this case the absorption and reduced scattering coefficients evaluated with the IAD program are verified through Monte Carlo simulations. If the the R and T obtained from the Monte Carlo simulation, with the coefficients from the IAD program as input, correlate to the IS measurement, then the evaluated coefficients are a good approximation of the real absorption and reduced scattering coefficients of the sample.

Firstly, the coefficients obtained by the IAD-program for the different samples were tested in the MCML program to ensure that they give the correct R and T, followed by a test of the coefficients that were chosen to represent the bulk material of the samples. In the simulations the LDPE was separated from the paperboard to give a more correct description of the samples. The problem in how to model the two different layers of paperboard, the white and the brown, still remains.

The reflectance and transmittance obtained by the MCML simulations corresponded very well with the IS-result, it only differ ± 1 percentage point for some of the samples, regarding both treated and untreated samples.

Untreated samples

Investigating the difference in reflection between the untreated samples, and linking this to the absorbed fraction, gives that $\Delta R = \Delta Abs$. That means that the extra fraction that is reflected by the white side is absorbed by the brown side. This was discussed in connection to the IS results in section 4.1 and is now supported by the MCML

simulations. The IS measurement resulted in a ΔR that was seven and thirteen percentage points for the thin and thick samples, respectively, at 805 nm. Comparing the difference in absorption in the MCML simulations yields the same numbers.

In the simulations the reflectance is divided into the two parts, specular and diffuse reflectance. The specular reflectance depends on the refractive index of the surface. It is 4 % for the LDPE coated surface and 2 % for the paperboard. This is off course based on the assumption that a weighted refractive index can be used for the paperboard. The diffuse reflectance is lower for the brown side compared to the white.

This means that a brown surface coated with LDPE gives the lowest reflection, but on the other hand it has a higher absorption and the transmission remains the same as for the white side.

Treated samples
In the case of the treated samples, the difference in reflection and absorption between the samples is much smaller, hardly noticeable. Only the difference in thickness affects the transmission and reflection.

Chosen coefficients
Since the samples have been investigated from both sides, the impact of the paperboard having two layers has been evaluated and coefficients to describe the bulk material have been chosen. These coefficients should describe the transmission properly, as discussed in section 4.2.3. Figures 4.15 to 4.18 show the transmission from the MCML simulations with the final coefficients together with the IS result.

The reflection of the white sides of the untreated samples do not correspond to the IS results, since the difference is bigger between the brown and white sides for those samples, and only the b-sides are considered when choosing the final coefficients.

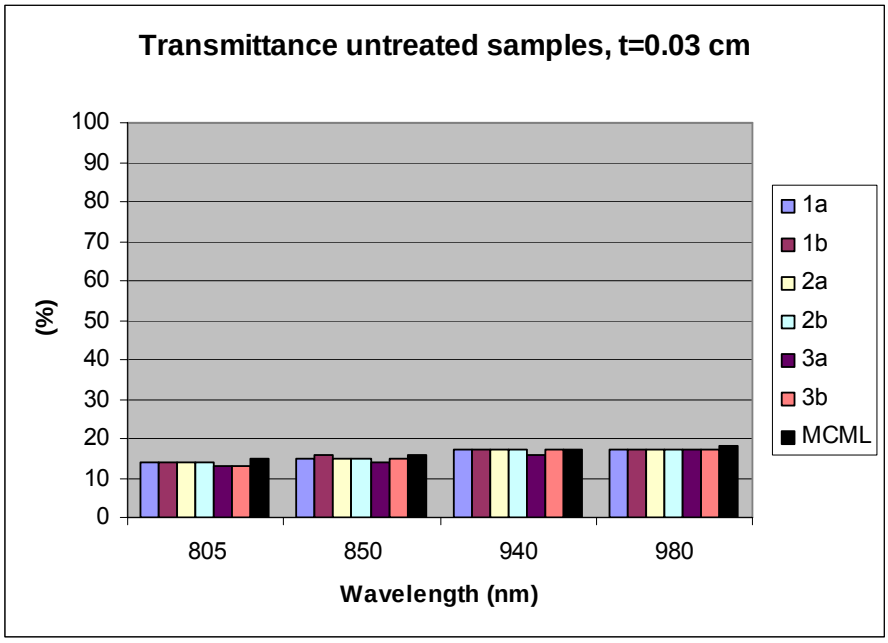

Figure 4.15. Comparison of the transmittance from the IS measurements and the MCML simulations with the final coefficients for the thin, untreated samples. The MCML results are slightly overestimated at shorter wavelengths.

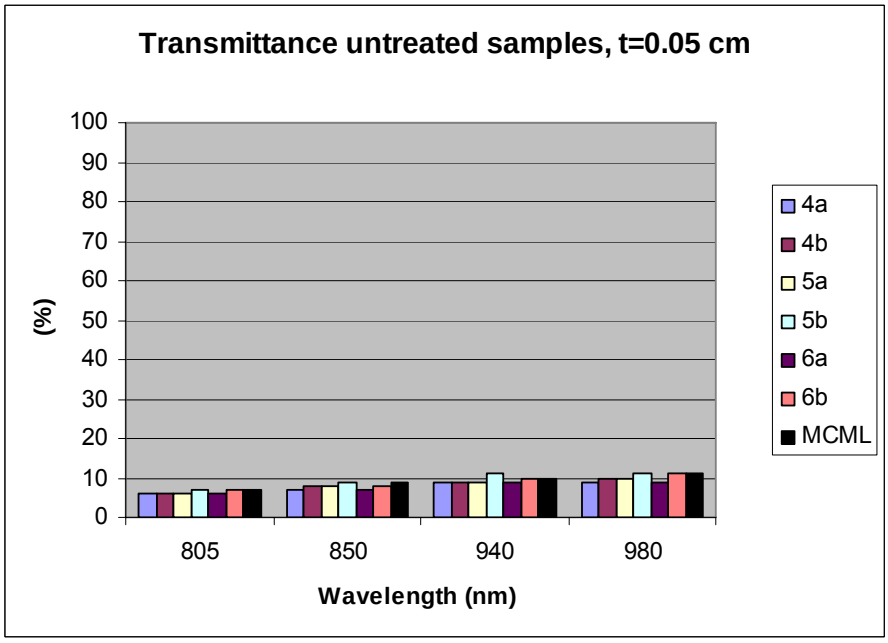

Figure 4.16 Comparison of the transmittance from the IS measurements and the MCML simulations with the final coefficients for the thick, untreated samples.

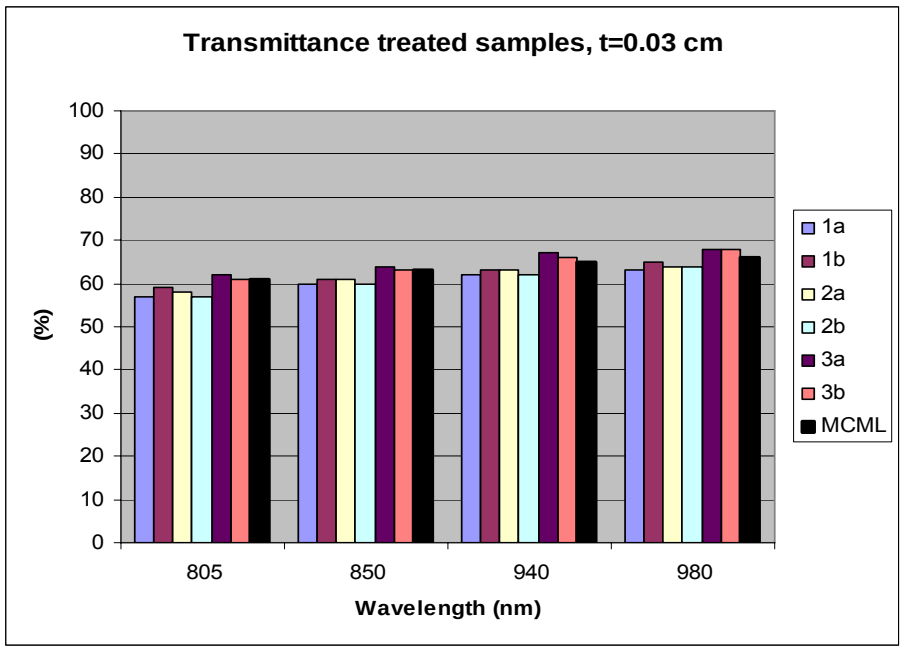

Figure 4.17 Comparison of the transmission from the IS measurements and the MCML simulations with the final coefficients for the thin, treated samples. The MCML results represent the transmission quite well throughout the wavelength range.

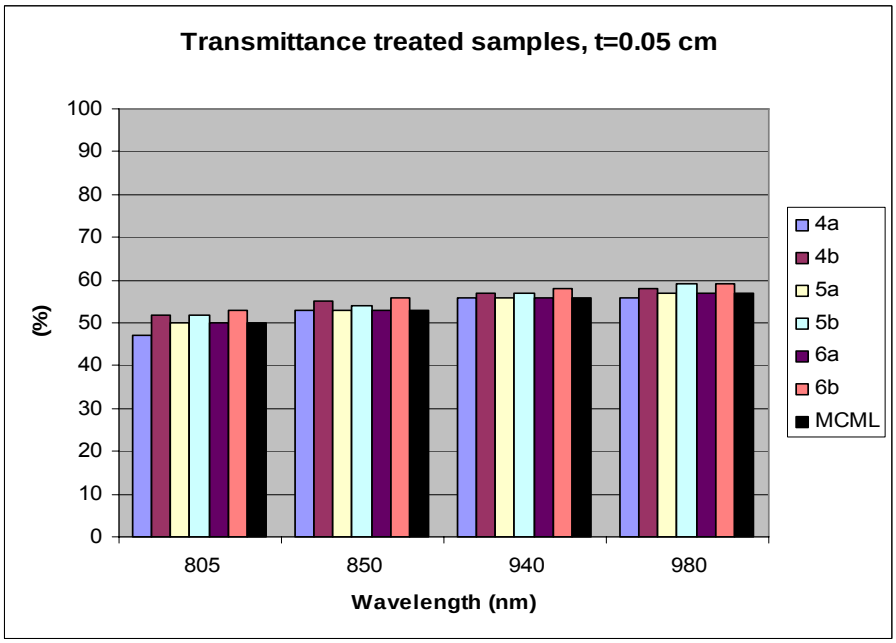

Figure 4.18 Comparison of the transmission from the IS measurements and the MCML simulations with the final coefficients for the thick, treated samples.

4.4 Modelling the light propagation

When the optical parameters are determined, different models can be applied to describe the light propagation through the samples. The two models used in this thesis are the diffusion model and a Monte Carlo program. The final coefficients described in section 4.2.3 are used in both simulation models.

Given the results of the reduced scattering coefficients of the different samples, it is clear that the diffusion equation will not be valid for the samples treated with oil.

These samples have reduced scattering coefficients of about 35 cm^{-1}, which makes the distance from the top surface to the location of the source, z_0, in the same range as the sample thickness, that is, the source will be placed in the bottom surface where the transmittance is to be calculated. In this case the light has no possibility to get scattered and become diffuse. Another model has to be applied and the Monte Carlo convolution program is chosen for these samples.

Regarding the untreated samples, the evaluated reduced scattering coefficient will result in a 10 times smaller distance from the surface to the source, and this is hopefully enough to obtain reliable results.

4.4.1 Untreated samples- Diffusion approximation

The light propagation through the untreated samples is modelled by the diffusion approximation of the time independent transport equation. The model is the one described in section 2.2.3 for the slab geometry. Six virtual point sources are used to simulate the laser light. Photon fluence are simulated as well as transmittance that is also compared to the IS results.

Figures 4.19 and 4.20 show the transmitted energy as a function of radius obtained from the diffusion simulation of the treated samples 3 and 6. Integrating the transmitted energy over the area yields a transmittance of 23 % for the thin sample and 11 % for the thick sample. From the IS measurement, the transmittance of the thin and thick samples is 8- 9 % and 16 %, respectively.

It is not surprising that the thick samples show a better agreement between the IS and diffusion results, because the condition for the diffusion approximations is that the light has been scattered and become diffuse. The probability for this to happen increases with the thickness of the sample. Considering the samples with thickness t=0.03 cm the transmittance is overestimated by the diffusion model because they simply are too thin.

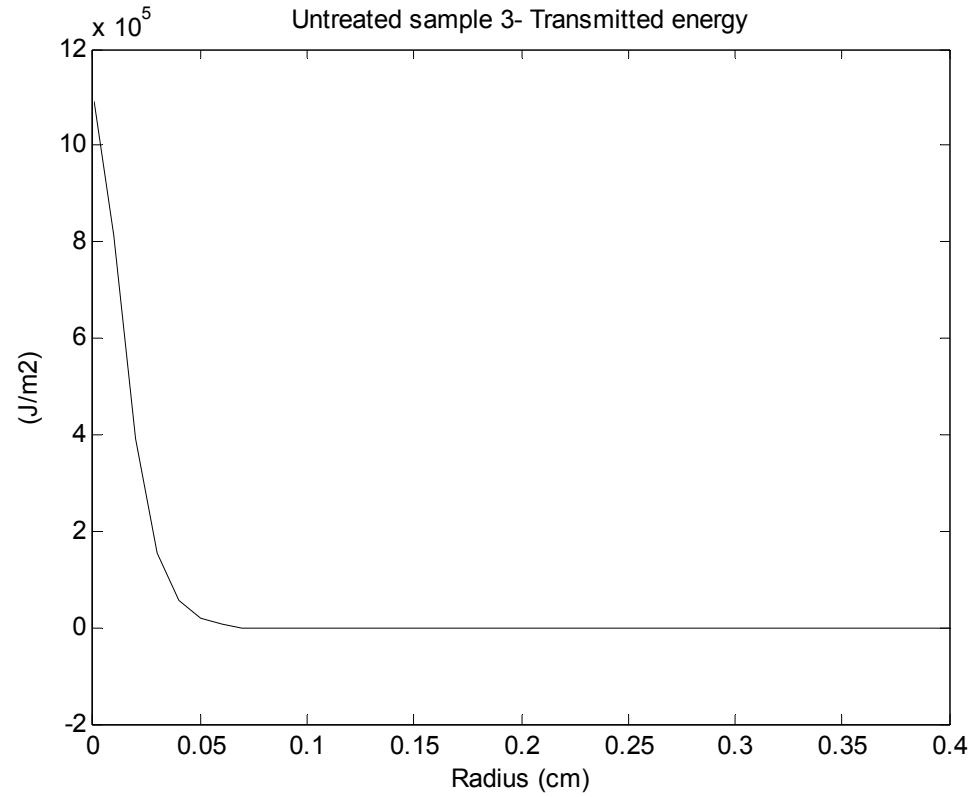

Figure 4.19 The transmitted energy of the untreated sample 3. When this curve is integrated over the area the transmittance is obtained, 23 % for this sample with thickness 0.03 cm.

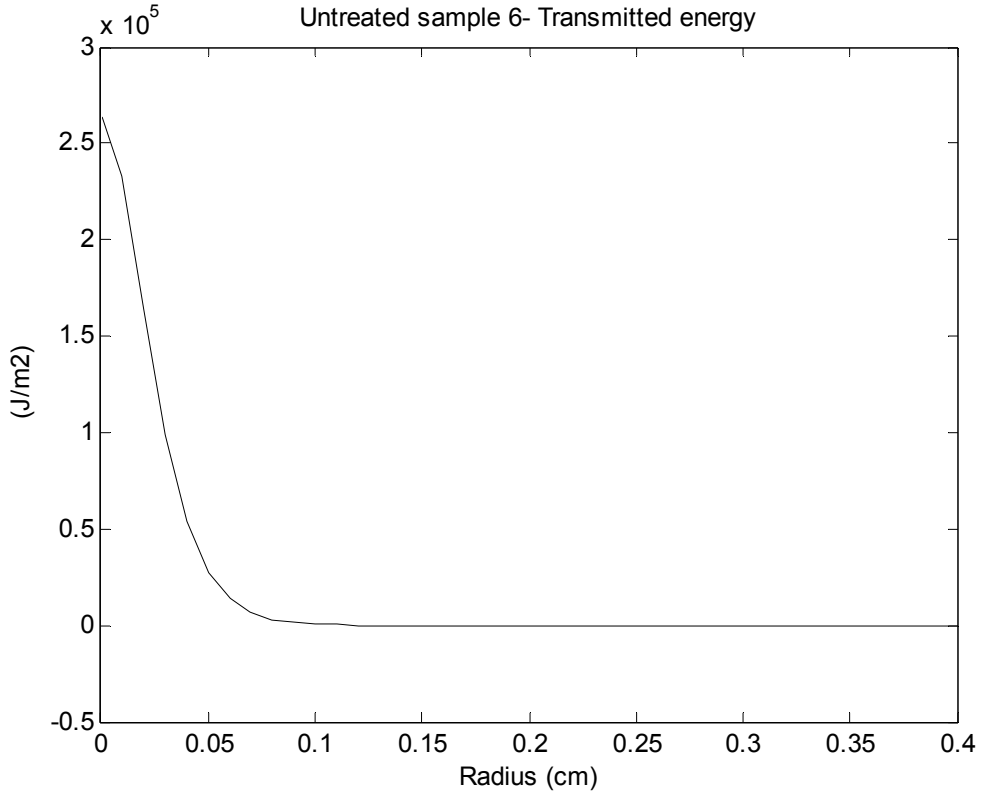

Figure 4.20 The transmitted energy of the untreated sample 6. When this curve is integrated over the area the transmittance is obtained, 11 % for this sample with thickness 0.05 cm.

4.4.2 Treated samples- CONV

CONV[31] is a program that convolutes the MCML simulation data to the input of a finite diameter photon beam. The input to the program is the information already given in the MCML together with the laser beam shape and power. In this case the incoming photons are in the shape of a flat beam with the radius 16 mm, which best approximates the beam shape of the Tetra Pak laser.

The input is 1 J on a surface with the radius 0.16 cm. The system is linear, so if the input is changed by factor n, the output is changed by the same factor.

For the sake of comparison, this model was applied to both untreated and treated samples, resulting in illustrations of how the oil affects the light propagation.

Figures 4.21 and 4.22 shows the simulated fluence through the untreated samples and figures 4.23 and 4.24 the fluence through the treated samples. The evaluated fluence through the treated samples shows peculiar disturbances that come from the simulation. Why this happens has not been figured out. If these disturbances are disregarded, the more probable appearance of a smooth fluence can be imagined in the figures.

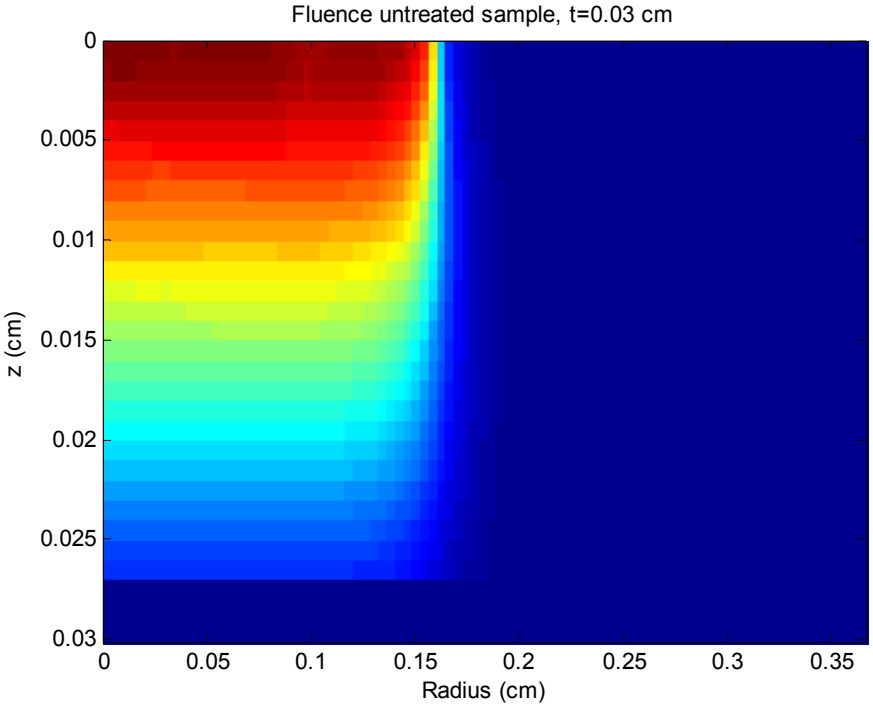

Figure 4.21 Fluence through the untreated sample 3. The thickness is shown on the y-axis. This sample has no LDPE coating and that is why the thickness is a bit smaller than 0.03 cm.

[31] L. –H. Wang, S. L. Jacques, L. –Q. Zheng (1997)

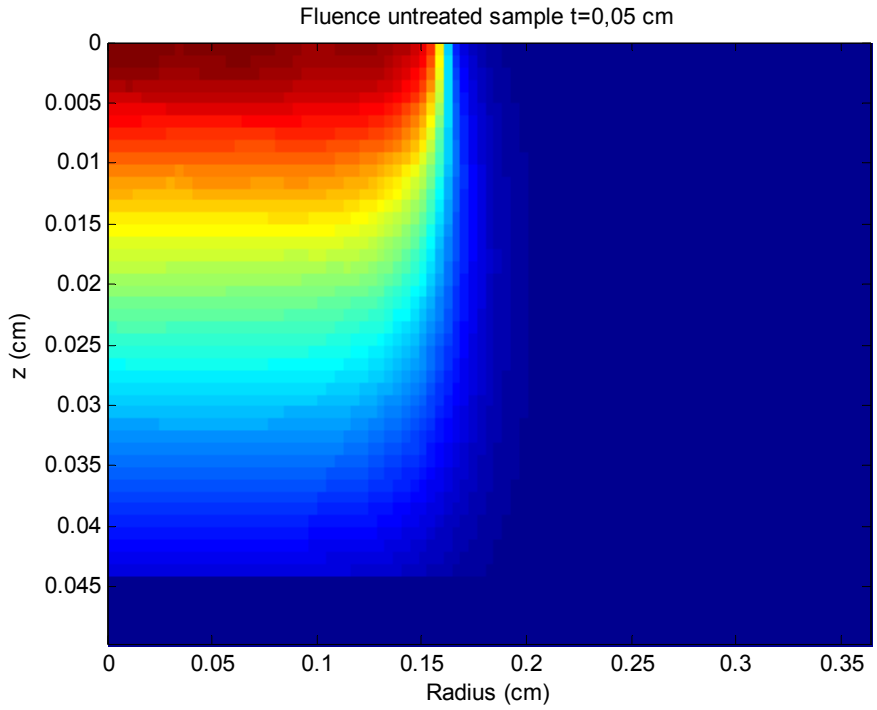

Figure 4.22.Fluence through the untreated sample 6. Because of the thickness being almost twice that of sample 3, the fluence has got more attenuated when reaching the bottom surface. This sample does not have the LDPE coating why the thickness is a bit smaller than 0.05 cm.

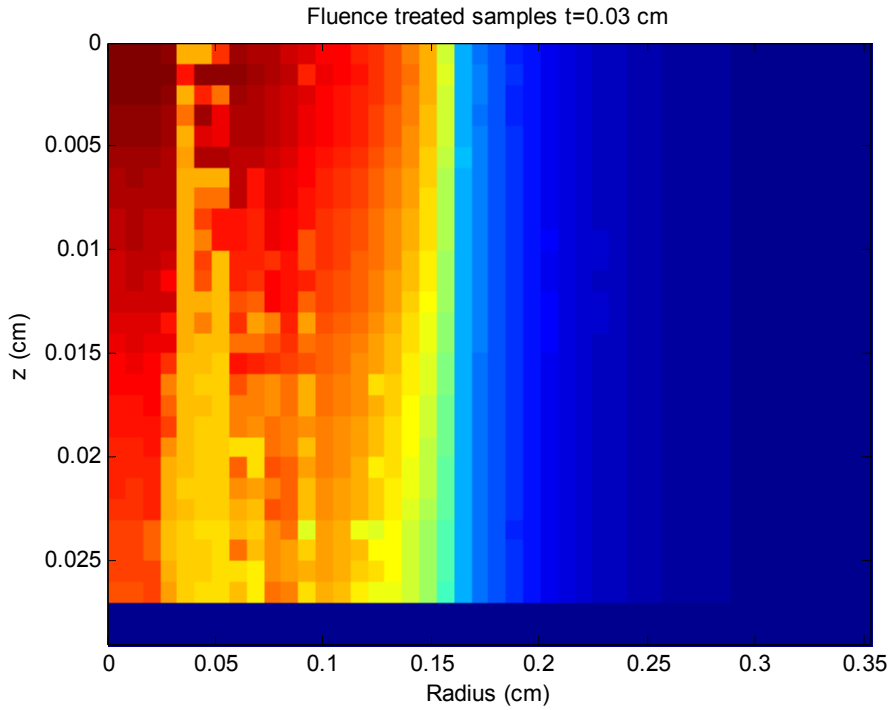

Figure 4.23 Fluence through the treated sample 3. Because of disturbances in the simulation, the evaluated fluence is not as smooth as that from the treated samples. However, if the disturbances are disregarded, the fluence has not been as attenuated at the bottom surface compared to the case with no oil treatment.

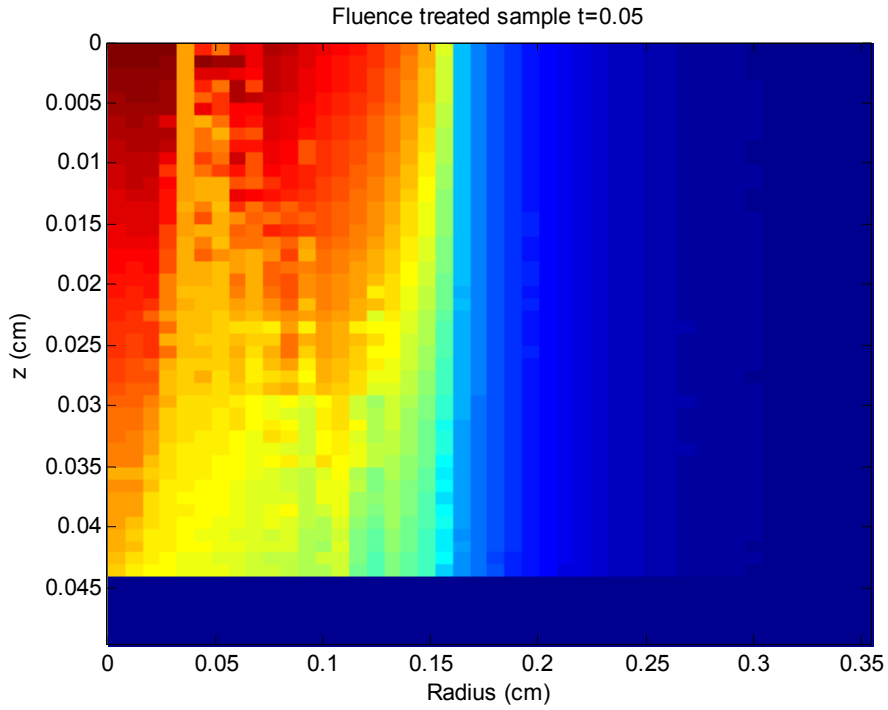

Figure 4.24 Fluence through the treated sample 6. Disregarding the disturbances, the fluence has not been as attenuated at the bottom surface compared to the case with no oil treatment.

Taking the natural logarithm of the fluence gives a curve that is smoother, and shows the slowly decaying fluence in the radial direction. For comparison, the logarithms of the fluence through the untreated as well as the treated sample are shown in figures 4.25 and 4.26.

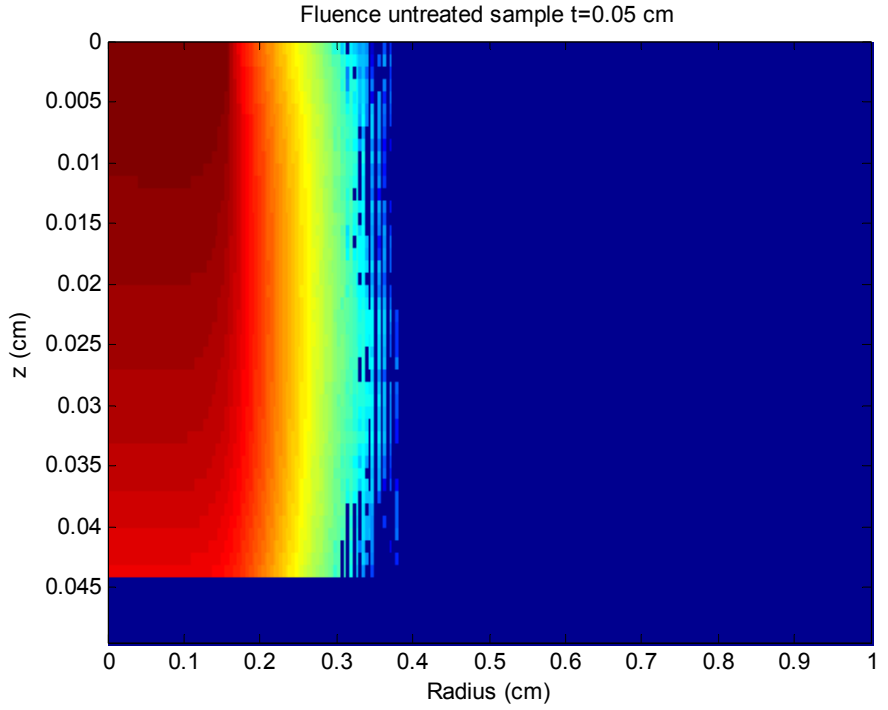

Figure 4.25. Logarithmic fluence through the untreated sample 6. To plot the fluence in a logarithmic scale shows the long tails of a very small fluence. In this case it is apparent that the fluence is attenuated rather fast.

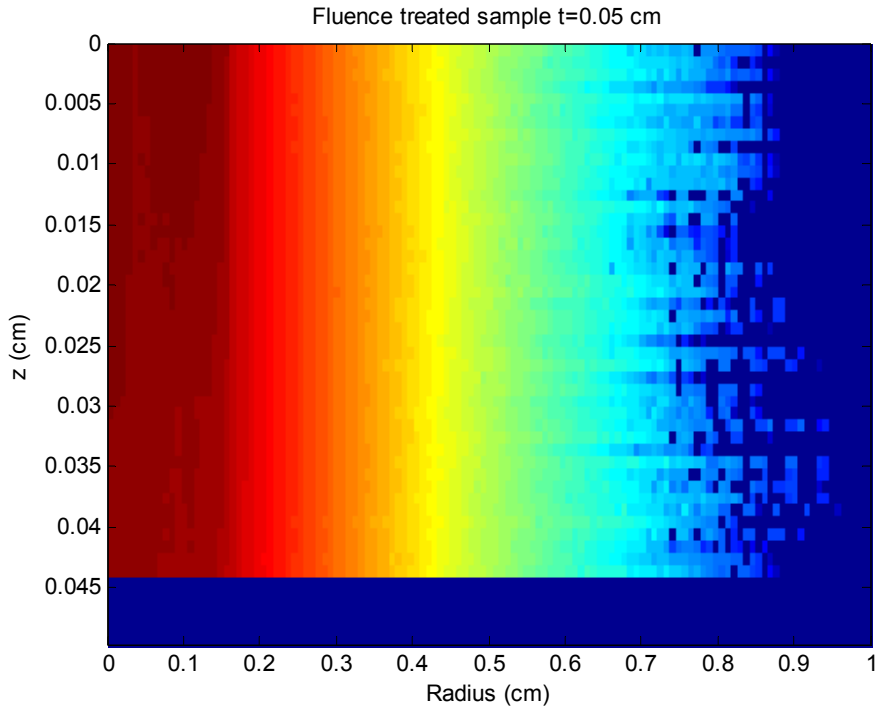

Figure 4.26 The natural logarithm of the fluence through the treated sample 6. The oil has facilitated the light propagation, especially in the z but also giving a longer tail in the radial direction.

The simulated transmittance as a function of radius is shown in figure 4.27 in the case of the untreated sample 3, and in figure 4.28 for the treated sample 6. Unlike the case in the diffusion model, the light source hits the sample over a surface and has the shape of a flat beam. The transmission curves with the radial dependence in the figures are obtained by dividing the output curve with the input energy. These results correlate well with the transmittance obtained form the IS measurements. The transmittance of the treated samples also shows disturbances.

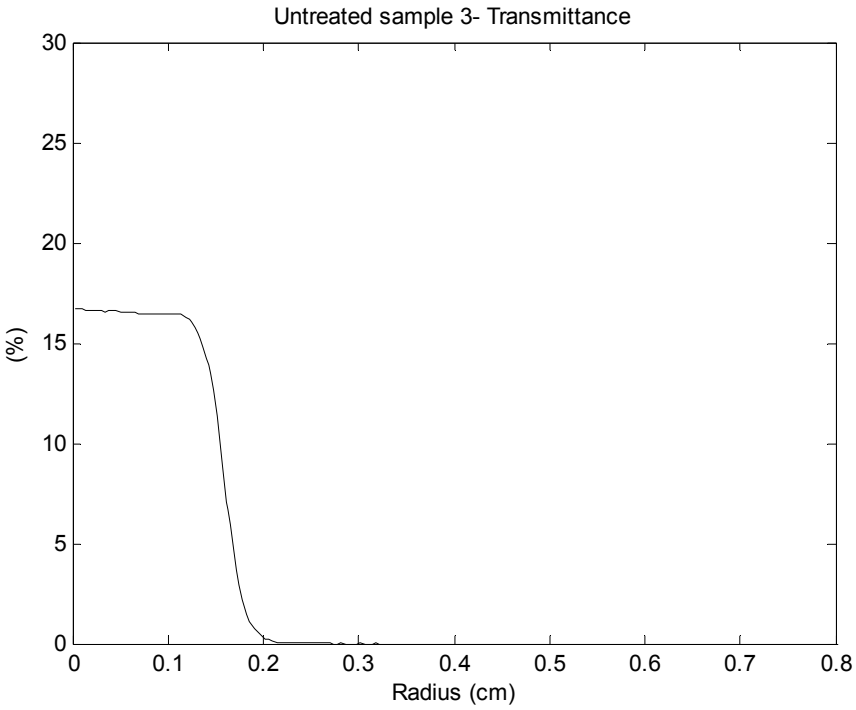

Figure 4.27. Simulated transmittance of the untreated sample 3. This transmittance is obtained regardless of which side is facing the light, since the set of coefficients has been chosen to describe the bulk material. The thickness of the sample is 0.03 cm.

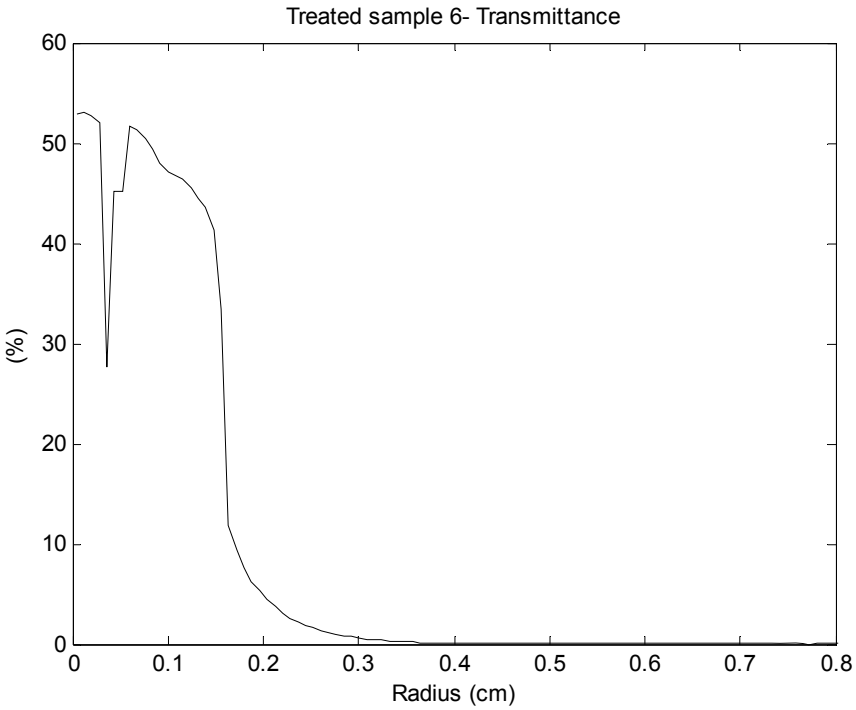

Figure 4.28. Simulated transmission of the treated sample 6. The thickness of the sample is 0.05 cm. This curve represents the transmittance of both sides, since the set of coefficients has been chosen that best describes the bulk material.

4.5 Experiments

The measurements done on Tetra Pak provided the result shown in figure 4.29, it shows how much laser power is needed to heat the carbon black with and without sample 6. The pyrometer controlling temperature is set to 180 °C. In the figure both sides of sample 6 is represented, showing that slightly less power is needed when the brown side, side b, is facing the laser. A measurement of the carbon black is also presented in the figure for a direct comparison. The difference between the two is the part that is reflected or scattered away from the measurement area, and not contributing to heating the carbon black.

Figure 4.30 show the transmittance of sample 6, and the results from all samples are presented in table 4.4.

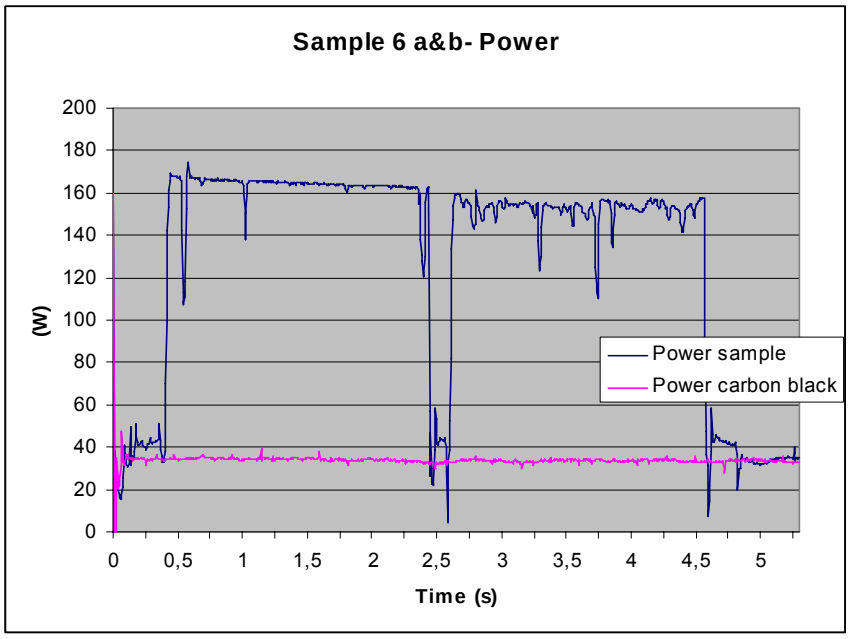

Figure 4.29 The required power to heat the carbon black to 180°C with and without the untreated sample 6 a and b. The a-side is shown between the times 0.5 to 2.5 s, the b-side between 2.5 to 4.5 s.

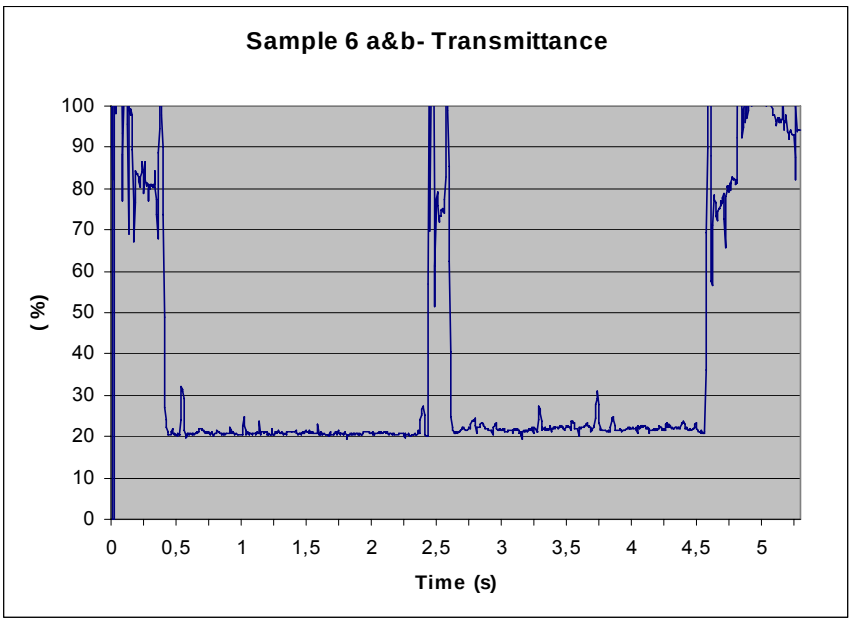

Figure 4.30 The transmittance of the untreated sample 6 a and b. The a-side is shown between the times 0.5 to 2.5 s, the b-side between 2.5 to 4.5 s.

The untreated samples have a transmittance of just above 20 %, the differences in thickness and surface properties have no measurable impact. When the samples are treated with mineral oil the difference in thickness appears in the measurements, the thin samples have a transmittance of about 55-60 % and the thick samples around 40-45 %. The differences between the samples are only one or a few percentage points, comparable to the difference in the IS measurements. In table 4.4, sample 5 has a lower P_{in} than samples 4 and 6, but with experience from earlier measurements this is not representative for sample 5 which generally has about the same values as 4 and 6.

Comparing the transmittances of the treated and untreated samples, the transmittance of the thin, untreated samples is almost 40% of the transmittance of the treated samples, and correspondingly 50% of the thick, treated samples.

Table 4.4 The results from the power measurements. The LDPE in the "Side facing laser" column indicates the surfaces with LDPE coating. Samples 1-3 have the thickness 0.03 cm and samples 4-6 have the thickness 0.05 cm.

		Untreated samples, P_{out}= 34 W		Treated samples, P_{out}= 34 W	
Sample	**Side facing laser**	**P_{in} (W)**	**Transmittance (%)**	**P_{in} (W)**	**Transmittance (%)**
1	a) White, LDPE	160	21	58	58
	b) Brown	155	22	63	54
2	a) White	164	22	62	54
	b) Brown, LDPE	157	22	60	56
3	a) White	163	22	56	60
	b) Brown	150	22	57	60
4	a) White, LDPE	167	21	81	41
	b) Brown	159	22	80	42
5	a) White	168	21	66	52
	b) Brown, LDPE	155	22	70	49
6	a) White	166	21	80	42
	b) Brown	152	22	83	40

Comparison IS and Tetra Pak results

Comparing the results from this measurement with the transmission obtained in the IS measurement, it is surprising to find that the transmission according to the TP measurements is actually higher for the untreated samples than the corresponding result from the IS measurement. Furthermore there is no difference depending on the thickness of the samples. The untreated samples on the other hand give a lower transmission in the TP measurement compared to the IS measurement. This is more realistic considering that it is the total transmission that is measured in the integrating sphere. In the Tetra Pak laser setup it is the temperature that is measured, and most likely there are some losses because the temperature is only measured in one spot.

Considering the untreated samples, it is doubtful that the pyrometer measures the temperature in the right spot since it doesn't register any difference between the thicknesses. In addition there is no sign of the LDPE melting when in contact with the carbon black film. LDPE has a melting point of 109-125 ºC[32] which makes it evident that the carbon black film has not reached the set temperature. This points towards the pyrometer measuring the temperature in another spot than assumed, or gets disturbed in some way.

When measurements are performed on the treated samples, the LDPE melts when it faces the carbon black film, indicating that the film has at least reached the LDPE melting temperature.

[32] Plasticsusa

Since the pyrometer measures the temperature and not the transmitted light, and because of the uncertainties with the measuring spot, it is difficult to compare these results with the IS measurements.

Chapter 5 Conclusions

The results from the IS measurements show that the different surfaces; brown or white, with or without LDPE-coating does not affect the transmission. However, the brown and white side affect the reflectance differently; the white side giving a higher reflectance than the brown. This is caused by a higher absorption in the brown paperboard and does not result in an increase in transmission.

The oil decreases the diffuse reflectance, the part that penetrates the surface of the sample but then is backscattered and leaves the sample at the same side as it entered. This means that it is not enough to treat the surface of the samples; the whole sample must be made more homogeneous to increase the transmission. Adding the oil makes the average transmittance increase from 16 % to 63 % for the samples with thickness 0.03 cm, from 8 % to 55 % for thickness 0.05 cm.

In the IAD evaluation model it is assumes that the samples are homogeneous; this is not the case why the samples are investigated from both sides to form an opinion of how this affects the obtained coefficients.

The IAD-simulation with only R and T as input gives the most reliable result, with reduced scattering coefficients around 200 times greater than the absorption coefficients for the untreated samples.

Adding oil to the samples has a positive impact on both the scattering and the absorption, making the reduced scattering coefficients decrease with a factor 10 for all samples and the absorption coefficients of the brown sides decrease to a level corresponding to the lower absorption in the white, untreated side.

Coefficients obtained from the brown, untreated are the most reliable and are assumed to describe the transmission correctly. Regarding the treated samples, coefficients obtained from both sides can be considered since the oil makes the difference between the samples very small.

Using the coefficients in the MCML program results in a transmission that corresponds very well to the IS results. These simulations also confirm that the difference in the surface reflectance is due to absorption in the brown paperboard.

The diffusion approximation handled light propagation through the thick, untreated samples rather well, but overestimates the transmission of the thin samples because they simply are to thin. The treated samples do not scatter the light enough for it to be diffuse why the Monte Carlo convolution program is a better choice to model the light propagation through those samples.

Regarding the untreated samples, the Tetra Pak measurements gave a higher transmittance than the one obtained in the IS measurements In addition, the carbon black has not reached the LDPE melting temperature that is lower than the set temperature, which makes it doubtful that the pyrometer measures the temperature in the assumed point on the carbon black. The results from the treated samples show a

more realistic result giving a transmission of 56 % and 42 % for the thin and thick samples respectively.

Since the pyrometer measures the temperature and not the transmitted light, and because of the uncertainties with the measuring spot, it is difficult to compare these results with the IS measurements.

Chapter 6 Acknowledgements

First of all, I want to thank my supervisor Hans Selberg and Tetra Pak Packaging Solutions AB for giving me the opportunity to do this thesis work. Hans Selberg was very supportive and enthusiastic throughout the project, and we had many interesting discussions.

I also want to thank a few persons at the Division of Atomic Physics, my co-supervisor Stefan Andersson-Engels for help and inspiration, Johan Axelsson and Arash Gharibi for the help with the integrating sphere measurements that turned out to be more problematic than I (or anyone) could imagine, and Jenny Svensson for introducing me to the IAD program.

Thanks to the staff at the department at Tetra Pak, especially Dag Svärd for getting me access to Matlab, Björn Böckerman for disturbing me in my slightly secluded office and off course Martin Andersson, Viveka Kronroth and Magnus Wijk for introducing the Friday breakfasts. This was greatly appreciated!

Last but not least, thanks to my friends and family for the constant encouragement.

Bibliography

1. A. J. Welch, M. J. C. van Gemert *Optical-Thermal response of laser irradiated tissue*, page 26, chapter 2, Plenum Press, New York (1995)

2. C. af Klinteberg ”On the use of light for the characterisation and treatment of malignant tumours”, Doctoral Thesis LRAP-245, Department of Physics, Lund Institute of Technology (1999)

3. S. Svanberg *Atomic and Molecular Spectroscopy,* Fourth Edition, Springer-Verlag, New York, Berlin, Heidelberg (2004)

4. C. af Klinteberg ”On the use of light for the characterisation and treatment of malignant tumours”, Doctoral Thesis LRAP-245, Department of Physics, Lund Institute of Technology (1999)

5. M. S. Thompson, “Photodynamic Therapy utilizing Interstitial Light Delivery Combined with Spectroscopic Methods”, Doctoral Thesis LRAP-331, Department of Physics, Lund Institute of Technology (2004)

6. J. Swartling “Biomedical and Atmospheric Applications of Optical Spectroscopy in Scattering Media”, Doctoral Thesis LRAP-290, Department of Physics, Lund Institute of Technology (2002)

7. S. Andersson-Engels, Tissue Optics http://kurslab.fysik.lth.se/FED4Medopt/diffusion2.pdf 2007-01-15

8. S. Andersson-Engels, Tissue Optics http://kurslab.fysik.lth.se/FED4Medopt/diffusion2.pdf 2007-01-15

9. J. S. Dam “Optical Analysis of Biological Media- continuous wave techniques”, Doctoral Thesis LRAP-265, Department of Physics, Lund institute of Technology (2000)

10. S. A Prahl et al. “Determining the optical properties of turbid media by using the adding-doubling method”, Applied optics, 32, 559-568 (1993)

11. J. Swartling “Biomedical and Atmospheric Applications of Optical Spectroscopy in Scattering Media”, Doctoral Thesis LRAP-290, Department of Physics, Lund Institute of Technology (2002)

12. S. A Prahl ”Optical Property Measurements using the Inverse Adding-Doubling Program” (1999) http://omlc.ogi.edu/software/iad/manual.pdf 2006-11-16

13. S. A Prahl et al.,”A Monte Carlo Model of Light Propagation in Tissue”, SPIE Institute Series Vol. IS 5 (1989)

14. S. A Prahl et al.,"A Monte Carlo Model of Light Propagation in Tissue", SPIE Institute Series Vol. IS 5 (1989)

15. Laser Physics, Lund Institute of Technology http://www-atom.fysik.lth.se/Kurser/FLaserfysik/Diodlab2002FysikEng.doc 2007-03-04

16. H. Ibach and H. Lüth, *Solid-State Physics- An Introduction to Materials Science*, Third edition, Springer-Verlag, Berlin, Heidelberg (2003)

17. S. Svanberg *Atomic and Molecular Spectroscopy*, page 228, chapter 8, Fourth Edition Springer- Verlag, New York, Berlin, Heidelberg (2004)

18. S. Svanberg *Atomic and Molecular Spectroscopy*, chapter 8, Fourth Edition, Springer- Verlag, New York, Berlin, Heidelberg (2004)

19. J.M Hollas, *Modern Spectroscopy*, page 351, chapter 9, Fourth edition, John Wiley & Sons Ltd., West Sussex (2004)

20. J.M Hollas, *Modern Spectroscopy*, chapter 9, Fourth edition, John Wiley & Sons Ltd., West Sussex (2004)

21. J.M Hollas, *Modern Spectroscopy*, page 352, chapter 9, Fourth edition, John Wiley & Sons Ltd., West Sussex (2004)

22. Plasticsusa http://www.plasticsusa.com/pe.html 2007-03-13

23. M Nogi, "Optically transparent bionanofiber composites with low sensitivity to refractive index of the polymer matrix", Applied Physics letters 87 (2005)

24. NIST Standard Reference Materials catalogue https://srmors.nist.gov/tables/view_table.cfm?table=204-2.htm 2007-02-20

25. Tissue Optics, Lund Institute of Technology http://kurslab.fysik.lth.se/FED4Medopt/ISlabhl.pdf 2006-11-15

26. Tissue Optics, Lund Institute of Technology http://kurslab.fysik.lth.se/FED4Medopt/ISlabhl.pdf 2006-11-15

27. J. R. Lorenzo, "Light Diffusion in Turbid Media with Biomedical Application", Instituto de Cienca de Materiales de Madrid, Madrid (2000) http://kurslab-atom.fysik.lth.se/FED4Medopt/JorgeR.pdf 2007-01-16

28. L. –H. Wang, S. L. Jacques, L. –Q. Zheng, "MCML- Monte Carlo modelling of photon transport in multi-layered tissues", Computer Methods and Programs in Biomedicine, 47, 131-146 (1995)

29. J. R. Lorenzo, "Light Diffusion in Turbid Media with Biomedical Application", Instituto de Cienca de Materiales de Madrid, Madrid (2000) http://kurslab-atom.fysik.lth.se/FED4Medopt/JorgeR.pdf 2007-01-16

30. C. N. Banwell, E. M. McCash, *Fundamentals of Molecular Spectroscopy*, chapter 3, Fourth edition, McGraw-Hill (1994)

31. L. –H. Wang, S. L. Jacques, L. –Q. Zheng, "CONV- Convolution for responses to a finite photon beam incident on multi-layered tissues", Computer methods and Programs in Biomedicine, 54, 141-150 (1997)

32. Plasticsusa http://www.plasticsusa.com/pe.html 2007-03-13

Appendix A Matlab code Diffusion theory

```
% Steady-state diffusion theory with six virtual sources
% slabsteady - Steadystate photon fluence as a function of r in a
slab geometry
%        (cylindrical symmetry)
%
% USEAGE: fluence=slabsteady(d,mus,mua,n,z,r,P)
%
% ARGUMENTS:
%   d   = slab thickness [m]
%   mus = reduced scattering coefficient [1/m]
%   mua = absorption coefficient [1/m]
%   n   = refractive index
%   z   = the depth where fluence is to be calculated
%   r   = a vector of the radius elements where fluence is to be
calculated [m]
%   P   = input power [W]
%
% OUTPUT:
%   fluence = a vector containing fluence data
function fluence=slabsteady(d,mus,mua,n,z,r,P)

% Speed of light
c0=3e8;
c=c0/n;

% Diffusion Theory (Extrapolated boundary)
% Determination of the distance ze. This depends on the difference
in
% refractive index between the two media

muc   = cos(asin(c/c0));
r0    = ((c0-c)/(c0+c))^2;
kappa = ((1-r0)*(1-muc*muc))/(1+r0+(1-r0)*muc*muc*muc);
diff  = 1/(3*(mus+mua));
ze    = 2*diff/kappa;

%z0 = distance from z=0 to tege point of the first source
%muf= Mu effective
z0   = 1/mus;
muf  = sqrt(3*mua*(mua+mus));
gamma=4*pi*mua;

%distances from the different sources to the measuring point
r1=sqrt((z-z0)^2+r.^2);
r2=sqrt((z+z0+2*ze)^2+r.^2);
r3=sqrt((z-2*d+z0-2*ze)^2+r.^2);
r4=sqrt((z-2*d-z0-4*ze)^2+r.^2);
r5=sqrt((z+2*d-z0+4*ze)^2+r.^2);
r6=sqrt((z+2*d+z0+6*ze)^2+r.^2);

% Calculate photon fluence W/m2
fluence=((P*muf^2)/gamma)*((1./r1).*exp(-muf*r1)-(1./r2).*exp(-
muf*r2)-(1./r3).*exp(-muf*r3)+(1./r4).*exp(-muf*r4)+(1./r5).*exp(-
muf*r5)-(1./r6).*exp(-muf*r6));
```

```
% steadyT - Steadystate transmittance as a function of r in a slab %
% % %geometry
%        (cylindrical symmetry)
%
% USEAGE: transmittance=steadyT(d,mus,mua,n,r,P)
%
% ARGUMENTS:
%   d   = slab thickness [m]
%   mus = reduced scattering coefficient [1/m]
%   mua = absorption coefficient [1/m]
%   n   = refractive index
%   r   = a vector of the radius elements where fluence is to be
calculated [m]
%   P   = power input [W]
%
% OUTPUT:
%   transmittance= a vector containing transmittance data [W/m2]

function transmittance=steadyT(d,mus,mua,n,r,P)

% Speed of light
c0=3e8;
c=c0/n;

% Diffusion Theory (Extrapolated boundary)
% Determination of the distance ze. This depends on the difference
in
% refractive index between the two media

muc   = cos(asin(c/c0));
r0    = ((c0-c)/(c0+c))^2;
kappa = ((1-r0)*(1-muc*muc))/(1+r0+(1-r0)*muc*muc*muc);
diff  = 1/(3*(mus+mua));
ze    = 2*diff/kappa;

% z0= distance from z=0 to the point of the source
% muf= Mu effective
z0   = 1/mus;
muf  = sqrt(3*mua*(mua+mus));

%distances from the different sources to the measuring point
r1=sqrt((d-z0)^2+r.^2);
r2=sqrt((d+z0+2*ze)^2+r.^2);
r3=sqrt((-d+2*d-z0+2*ze)^2+r.^2);
r4=sqrt((-d+2*d+z0+4*ze)^2+r.^2);
r5=sqrt((d+2*d-z0+4*ze)^2+r.^2);
r6=sqrt((d+2*d+z0+6*ze)^2+r.^2);

%Calculate diffuse transmittance
% z=d
no1=(1./r1+muf).*((d-z0)./r1.^2).*exp(-muf*r1);
no2=(1./r2+muf).*((d+z0+2*ze)./r2.^2).*exp(-muf*r2);
no3=(1./r3+muf).*((-d+2*d-z0+2*ze)./r3.^2).*exp(-muf*r3);
no4=(1./r4+muf).*((-d+2*d+z0+4*ze)./r4.^2).*exp(-muf*r4);
no5=(1./r5+muf).*((d+2*d-z0+4*ze)./r5.^2).*exp(-muf*r5);
no6=(1./r6+muf).*((d+2*d+z0+6*ze)./r6.^2).*exp(-muf*r6);

transmittance=(-P/(4*pi))*(-no1+no2-no3+no4-no5+no6);
```

```
% Steady state transmittance through the slab
% Prov 3

R=0:0.0001:0.004;
T805=steadyT(0.00027,34500,175,1.324,R,1);
T850=steadyT(0.00027,35570,113,1.324,R,1);
T940=steadyT(0.00027,36880,54,1.324,R,1);
T980=steadyT(0.00027,37510,40,1.324,R,1);

% Average transmittance considering all four wavelengths

T=(T805+T850+T940+T980)./4;
figure(1)
plot(R,T)
title('Sample 3- Transmitted energy');
xlabel('Radius (m)');
ylabel(' (J/m2) ');

% Integrating over the area to obtained total transmitted
energy/power

T_tot=0;
for i=1:length(T)-1;

    T_tot=T_tot+pi*(R(i+1)^2-R(i)^2)*T(i);
end
```

Appendix B Summary in Swedish

Bestämning av de optiska egenskaperna hos material för laserapplikationer.

A. Nordström

Bakgrund och syfte

Tetra Pak är ett världsledande företag inom process och förpackningsindustrin, som hela tiden jobbar för att utveckla nya tekniker som samtidigt är förenliga med nyckelfrasen ”En förpackning ska spara mer än den kostar”. Detta ställer höga krav både då det gäller ekonomi och miljö. Huvudkomponenten i förpackningar, kartong, består av cellulosa och stämmer väl på båda aspekter.

Syftet med denna undersökning är att bestämma kartongens optiska egenskaper för laserapplikationer. Det är intressant att se hur en behandling av kartongen kan påverka dessa egenskaper, i detta fall handlar det om en olja som tränger in i kartongen. Kartongprover med olika ytor och tjocklekar undersöks för att se hur detta påverkar reflektion och transmission.

Teori

De parametrar som används för att beskriva ett prov är absorptionskoefficienten, μ_a, spridningskoefficienten, μ_s och anisotropifaktorn, g. Absorptions- och spridningskoefficienterna beskriver en sannolikhet att en inkommande foton ska absorberas resp. spridas under en längdenhet och anges i cm^{-1}. Anisotropifaktorn är ett mått på hur spridningen är riktad, och har värden i intervallet -1 till 1, där -1 beskriver bakåtspridning, 0 isotropisk spridning, dvs. att spridingen sker lika mycket i alla riktningar och 1 innebär framåtspridning. I vissa fall kan inte g och μ_s bestämmas var för sig och då används istället den reducerade spridningskoefficienten $\mu_s'=(1-g)\mu_s$.

Utförande

Provernas reflektans, R, transmittans, T, samt den kollimerade transmittansen T_{col}, bestämdes genom mätningar i en integrerande sfär, IS.

Med ett utvärderingsprogram baserat på adding-doubling metoden, IAD, bestämdes de optiska parametrarna μ_a, μ_s och g. Då mätningen av T_{col} är svår att genomföra korrekt, är en utvärdering utan denna mer tillförlitlig. Då erhålls istället μ_s' samt μ_a. Dessa koefficienter testades sedan med ett Monte Carlo program för att se om de gav samma R och T som IS, alltså om koefficienterna ger en bra beskrivning av proverna.

Ljustransporten genom kartongproverna modellerades med diffusionsapproximationen i fallet med obehandlad kartong, och med ett Monte Carlo program för de oljebehandlade proverna. Diffusionsteori baseras på att ljuskällan approximeras med en isotropisk punktkälla på avståndet $z_0=1/\mu_s'$ in i provet, och att ljuset antas vara diffust när det når detektorn. Monte Carlo programmet simulerar transmissionen av en inkommande ljusstråle med bestämd radie och intensitetsfördelning.

Resultat och diskussion

IS-mätningen gav olika reflektans beroende på vilken yta som är vänd mot ljuset, vit sida reflekterar mer. Transmittansen påverkades dock inte av detta, vilket tyder på att minskningen i reflektans för den bruna sidan beror på absorption. IAD- simuleringarna gav en μ_s' som var ca 200 gånger större än μ_a för de obehandlade proverna, vit sida ledde till högre μ_s' och lägre μ_a än brun.

Oljan gjorde att spridningen minskade markant, μ_s' blev ca 10 gånger mindre. Absorptionen minskade för de bruna sidorna och blev i nivå med absorptionen i de vita. Det är viktigt att komma ihåg att proverna utvärderas med antagandet att de är homogena, vilket inte är fallet i verkligheten. Detta gör att de utvärderade koefficienterna får ses som den bästa

möjliga approximationen. Figur 1 visar transmissionen av de obehandlade, tunna proverna från IS-mätningen. Prov 1-3 har tjockleken 0.03 cm och 4-6 tjockleken 0.05 cm. Därtill representerar ett a en vit sida mot ljuskällan, och b en brun sida mot ljuskällan. Förutom detta har prov 1a och 2b en plastbeläggning.

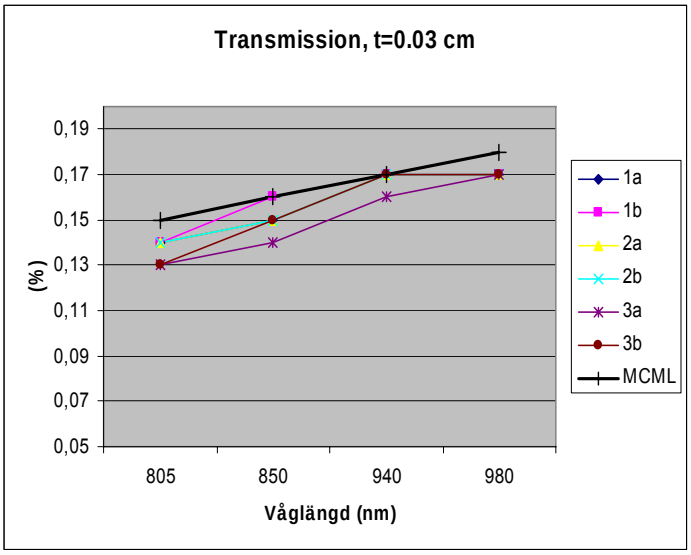

Figur 1. Transmissionen från de obehandlade, tunna proverna. Jämförelse mellan IS och MCML resultat.

Eftersom proverna är gjorda av samma material, borde de beskrivas av samma koefficienter. De koefficienter som bäst beskriver transmissionen testades med Monte Carlo simuleringar och resultatet från dessa visas också i figurerna. Figur två visar resultatet från IS och MCML för de behandlade proverna. Oljan innebär en markant ökning av transmissionen. Proverna med tjocklek 0,05 cm hade en lägre transmission, ca 10 % för obehandlat och 55 % med olja.

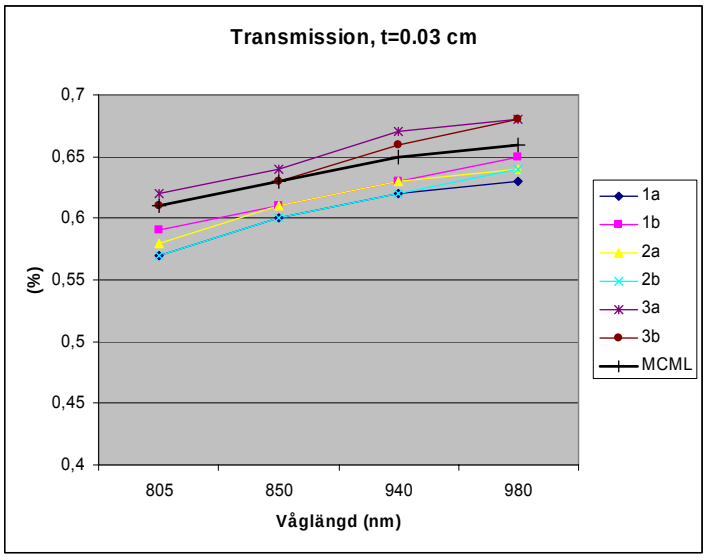

Figur 2. Transmissionen från de behandlade, tunna proverna. Jämförelse mellan IS och MCML resultat.

Simuleringar enligt diffusionsmodellen utfördes på de obehandlade proverna och resulterade i transmittanser som stämde väl med IS resultatet för de tjocka proverna, men lite sämre för de tunna. Detta beror på att ljuset inte hinner spridas och bli diffust om provet är för tunt Att

ljuset är diffust är ett villkor för att diffusionsmodellen ska vara giltig. De behandlade provernas transmittans simulerades med ett Monte Carlo program, som också gav resultat jämförbara med IS mätningen. Här simulerades även fotonflödet genom proverna, också för de obehandlade, vilket visas i figur 3 för ett tunt, obehandlat prov.

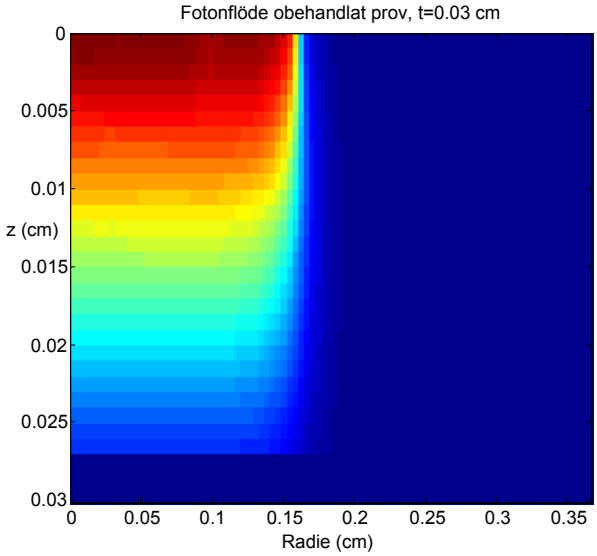

Figur 3. Fotonflödet genom ett obehandlat prov utan plastbeläggning, t= 0.03 cm.

Slutsats

Oljan minskar den diffusa reflektansen, den del som penetrerat ytan och som sen genom bakåtspridning lämnar provet på samma sida som den kom in. De olika ytorna har ingen betydelse för transmittansen, vilket innebär att hela provet måste behandlas och bli mer homogent, att ytbehandla räcker inte.

Oljan har en positiv effekt på både spridningen och absorptionen då den minskar den reducerade spridningskoefficienten med ca en faktor 10 för samtliga prover och sänker absorptionskoefficienten för den bruna sidan till samma nivå som den lägre absorptionen i den vita, obehandlade sidan.

Koefficienterna som valdes att representera provernas optiska egenskaper gav en bra beskrivning av transmittansen, testat med Monte Carlo simuleringar. Diffusionsmodellen är giltig för de tjocka obehandlade proverna men de med tjocklek 0.03 cm är något för tunna för att ljuset ska hinna spridas och bli diffust.